UNIVERSITAT POLITÈCNICA DE CATALUNYA
BARCELONATECH
Escola Superior d'Enginyeries Industrial, Aeroespacial i Audiovisual de Terrassa

AERODYNAMIC STUDY OF THE WAKE EFFECTS ON A F1 CAR

Author:
Alex Guerrero Lorente

Director:
Roberto Castilla Lopez

Final Dissertation

Bachelor's degree in Aerospace Vehicle Engineering

Escola Superior d'Enginyeries Industrial, Aeroespacial i Audiovisual de Terrassa
Universitat Politècnica de Catalunya

30th of June 2020

Contents

List of Figures

List of Tables

Nomenclature

Acronyms and abbreviations

CAD	Computer Aided Design
CFD	Computational Fluid Dynamics
CoP	Center of Pressure
CS	Control Surface
CV	Control Volume
DRS	Drag Reduction System
F1	Formula One
FB	Front Balance
FIA	Federation Internationale de l'Automobile
FVM	Finite Volume Method
GCI	Grid Convergence Index
PI	Point of Inflection
RANS	Reynolds-averaged Navier–Stokes equations

Dimensionless numbers

Ma	Mach number
Re	Reynolds number

y+ y Plus

Symbols

δ Boundary layer thickness [m]

μ Dynamic viscosity [kg/m $\cdot s$]

ν Kinematic viscosity [m^2/s]

ρ Fluid density [kg/m^3]

τ Shear stress [Pa]

$\vec{n}$ Surface normal unit vector

a Sound velocity [m/s]

C_D Drag coefficient

C_f Friction coefficient

C_L Lift coefficient

C_p Pressure coefficient

D Drag Force [N]

E Efficiency

g Gravitational acceleration [m/s^2]

L Lift Force [N]

l Reference length [m]

m Mass [kg]

P Fluid Pressure [Pa]

S Reference surface [m^2]

t Time [s]

U_∞ Fluid Velocity [m/s]

V Volume [m^3]

Acknowledgments

Firstly, I would like to thank my supervisor **Roberto Castilla** for accepting the idea of this project and the guidance that he has provided.

En segundo lugar, agradecer a mi **familia** el apoyo incondicional que me han dado siempre, fuera cual fuese la situación y siempre confiando en mí.

To my family and friends,

Declaration of honor

I declare that,

the work in this Degree Thesis is completely my own work,

no part of this Degree Thesis is taken from other people's work without giving them credit,

all references have been clearly cited,

I understand that an infringement of this declaration leaves me subject to the foreseen disciplinary actions by the **Universitat Politècnica de Catalunya - BarcelonaTECH.**

Abstract

Formula One will see one of its main revolutions in terms of design with the **future 2022 regulations**, which are mainly based on a **simplified aerodynamic package** that will allow the closer racing that the current regulations are said to be unable to meet.

The present study is based on the **evaluation and quantification** of the **aerodynamic performance** on a 2017 spec. adapted **F1 car** —the latest major aerodynamic update— by means of a *CFD* study. Both free **stream and flow disturbance conditions** are evaluated in order to study and quantify the effects that the **wake** may cause on the latter case.

The *CFD* techniques are primarily selected as other resources —such as the usage of a wind tunnel or any other experimental solutions—, are currently out of reach to deal with such a study. However, as the *CFD* discipline involves a rather strict and accurate process to be able to deal with external aerodynamic problems, the methodology is accepted in order to **discern whether the current F1 regulations require an urgent change** in terms of aerodynamic designs.

Objective

The main objective of this project is to **evaluate, study and numerically quantify** the aerodynamic performance of a 2017 spec. adapted F1 car in order to **argue** whether the 2022 changes in the regulations **are somehow justified** in terms of **aerodynamic necessities**.

Scope

The present study is aimed at covering the following points:

1. State of the art: A general background about Fluid Mechanics and a **broad glance of the main aerodynamic packages and designs** is offered in order to familiarise the reader with the nomenclatures and the history of aerodynamics in F1. Moreover, a brief introduction of the **modern techniques** used to quantify numerically the aerodynamics of F1 cars is also offered, emphasising on the importance of CFD techniques.

2. Simulation and performance of a F1 car: This chapter is based on the CFD preparation of a F1 2017 spec. car and eventually the **simulation of the different cases** both in free stream conditions and under wake flows.

3. Results and evaluation: A review of the numerical results is obtained in order to **quantify in both of the simulation cases the aerodynamic performance** encountered. **Qualitative results**, such as streamline plots and pressure distribution are also attached to help the reader understand the results obtained. Finally, a conclusion regarding the data obtained is reached as stated initially.

4. Economic impact of the project: Quantification of the **main economic weight that the project** implies in order to determine the real cost of itself.

5. Organisation and planning: General view of **how the project is structured, scheduled and planned** since the beginning and origin of the idea to the final delivery.

6. Conclusions: A compendium of **statements and final decisions regarding the results gathered** with the whole study performed. These include an answer to the main objective's questions provided with the obtained evidence and a logical reasoning.

7. Future works: A brief comments on the **possible future works** regarding the improvement of this project are presented. This includes the proposals of new in-depth studies as well as modifications within the current one.

As for the limitations and out-of-scope matters, it is important to state that only the **RANS k-w SST** turbulence models are studied and that the maximum mesh size is limited **40M elements** due to computational restrictions.
Moreover, this is a CFD study, which means that its reach does not exceed the computational boundaries, so **no experimental analysis** —by means of wind tunnel testing— are conducted.

Requirements

In order to execute this study, the usage of the appropriate software is required. The software selected for the simulation procedures and post-process visualisation is free of any economical cost. In general traits, the requirements of this project in order to be able to fulfil the scope of the study are:

- Download of the required software licenses and creation of user accounts. In this case, the software needed is *Salome-Meca* to modify and clean-up the geometries, although a student license of *Solidworks* is also used. Both accounts in *Simscale* and *Onshape* to simulate the cases and the post-process viewer *Paraview*. However, a *Matlab* license is also useful for data processing purposes.
- Knowledge of the above stated software so as to be able to perform the the modifications on the geometry, the simulation and the post-process visualisation.
- Basic knowledge of Fluid Mechanics, in order to understand the mathematical background of any process as well as the interpretation and elucidation of the results obtained.

Motivation and Justification

Ever since I was a kid I have always felt passionate about motorsport and especially its technical side. That way, I have always been thrilled by trying to **figure out how engineers scratch their heads in order to make the flow around F1 cars behave the way they desire**, of course, to get a better performance. For this reason, I truly believe that Computational Fluid Dynamics –*CFD*– techniques are **essential to understand these phenomena**, and, in addition to the little education we receive, I personally reckon it is appropriate to carry out this project to expand my knowledge and interest regarding this matter.

For years, it has been openly stated that F1 has lost much of its spectacular nature due to the difficulty of the cars to be able to follow each other closely for a long period of time. The chasing of the leading car has been **severely compromised by the sophisticated aerodynamics of these single-seater cars** —mostly due to the turbulent wake generation and clearly disturbed flow—. This way, I find it rather convenient to **numerically analyze and quantify the actual loss of aerodynamic loads on a F1 car** due to the immediate presence of a rival in front of it and then, establish a fair comparison with the situation of a free stream condition.

Part I

Introduction

Chapter 1

Fundamentals of Fluid Mechanics and Aerodynamics

"Truth is ever to be found in simplicity, and not in the multiplicity and confusion of things."

- Sir Isaac Newton, *Philosophiæ Naturalis Principia Mathematica, 1687.*

This first chapter intends to orient the reader about the very **fundamental basis of Fluid Mechanics** and **Aerodynamics** in order to be able to follow adequately the development of the present work.

1.1 Fluid definition

From a Fluid Mechanics point of view, matter can be presented in two possible and different states: **Fluid and Solid**. The main contrast between them is found in the way **they behave against a shear stress**, which is defined as the ratio between the component of the force tangent to a certain surface and its area [24]. That shear stress is found in the limit of this ratio as the area is reduced to a single point as seen in Equation 1.1.

$$\tau = \lim_{\triangle A \to 0} \frac{\Delta F_t}{\triangle A} \tag{1.1}$$

A fluid is a substance that **suffers a deformation** when it is subjected to a certain effort, no matter how small it is. These substances are divided depending on the relative separation between the molecules and the forces that keep them altogether into liquids or gases [2]. The latter ones are characterized by having its molecules quite distant from each other and rather low attractive forces, therefore they have the capacity to occupy the whole volume in which they enclose. Liquids, on the other side, have higher attraction forces and a smaller longitude between molecules so they have a natural tendency to keep their volume.

1.2 Flow Stationarity

A flow is defined as the movement of a certain fluid, usually defined by physical variables just like its pressure, velocity or temperature for each fluid point. If this set of variables is constant over time, the flow is defined as a **stationary flow**. In such case, the fluid particles will move along the current line that follows through that point [24].

A **non-stationary flow** behaviour is characterised by being its characteristic variables not constant over time. This way, the streamlines can change its direction, which allows the same particle to follow a different streamline at every instant.

1.3 Laminar and Turbulent flows

A flow is considered **laminar** when the movement of the fluid is **ordered, layered and smooth**. In a laminar flow, the fluid moves in parallel layers without mixing and each fluid particle follows a smooth path through the streamlines.

On the other hand, **turbulent** flows are such whose fluid movement occurs in a **chaotic way**, in which the particles move disorderly and their trajectories are found forming small periodic swirls, not coordinated [25]. Due to this, the trajectory of a particle can be predicted up to a certain scale, from that on, the trajectory of the particle is unpredictable, more precisely, chaotic. Figure 1.1 pretends to show the difference of these 2 regimes.

Mathematically, a flow regime can be determined by the so-called **Reynolds Number**, *Re*, which is a dimensionless magnitude that dictates whether the flow is laminar or turbulent as seen in Equation 1.2. This magnitude can be understood as the ratio of inertial and viscous forces.

$$Re = \frac{\text{Inertial forces}}{\text{Viscous forces}} = \frac{UL}{v} \tag{1.2}$$

Where U represents the flow velocity, L is the characteristic length and v is the kinematic viscosity of the fluid.

This way, for values of *Re* below a certain **critical value**, the viscous forces will dominate against the inertial ones and the flow will have a laminar behaviour. If this value is higher than that critical Reynolds number, the flow will be turbulent. This critical value depends on the physics of each case, so it **cannot be considered a universal frontier**.

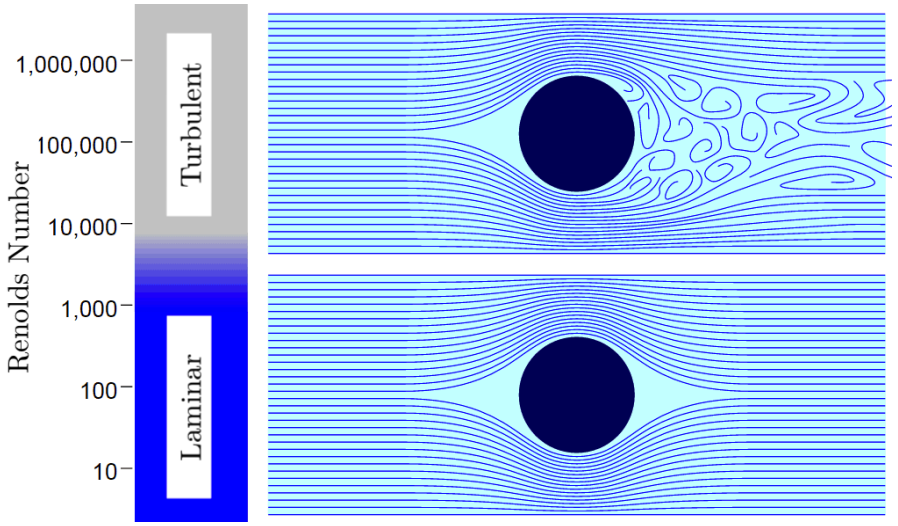

Figure 1.1: Laminar and Turbulent flows. Courtesy of Reactor Pysics [1].

1.4 Compressible and incompressible flows

A **compressible** flow is the one whose **density values change** over the domain, while an **incompressible** flow is defined as one whose **density remains constant**. The mathematical criteria for analysing whether a flow is compressible or

incompressible is the **Mach number** [24]. This dimensionless magnitude relates the velocity U_∞ of the fluid with the velocity of the sound in that fluid a, as seen in Equation 1.3.

$$Ma = \frac{U_\infty}{a} \tag{1.3}$$

Hence, a distinction is performed between wide ranges of the Mach number to **classify** the flows [2]:

- Ma $<$ 0.3: **Incompressible** flows, the density changes are insignificant.
- 0.3 $<$ Ma $<$ 0.8: **Subsonic** flows, the density changes are substantial but no shock waves appear.
- 0.8 $<$ Ma $<$ 1.2: **Transonic** flows, the shock waves start to appear noting supersonic and subsonic regimes on the flow.
- 1.2 $<$ Ma $<$ 3.0: **Supersonic** flows, shock waves are present although there is usually a subsonic section close to the leading edge.
- 3.0 $<$ Ma: **Hypersonic** flows, strong shock waves phenomena and other flow changes are present.

1.5 Boundary Layer

In fluid mechanics, the **boundary layer** of a fluid is the area where its movement is disturbed by the presence of a solid which is in contact with. The boundary layer is understood as one in which the speed of the fluid with respect to the moving solid **ranges from zero to 99 %** of the speed of the undisturbed current U_∞. Figure 1.2 shows a free stream flow with a speed U_∞ which encounters a flat plate of distance L. As there is a non-slip condition, the flow is slowly decelerated as it makes contact with the flat plate. This way, a **velocity gradient** appears due to the shear forces between the fluid layers close to the plate and those far away [2].

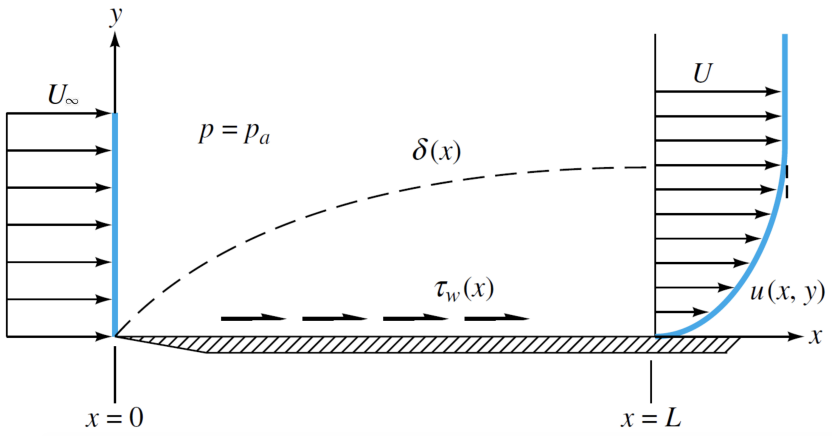

Figure 1.2: Boundary layer visualisation on a flat plane. Extracted from [2].

1.5.1 Boundary Layer separation

The separation of the mentioned boundary layer is a critical phenomena that occurs in external flows in aerodynamics. When this effect occurs, **the flow is detached from the surface** of the solid causing the the separation of the boundary layer [26]. This might be caused by the loss of momentum close to the wall due to the movement of the fluid downstream that finds an adverse pressure gradient —see Figure 1.3 — or by a sudden sharp change in the physical geometry.

To be able to understand that, in an adverse gradient, the second derivative of the velocity is greater than zero at the wall, so it must be negative at the outer layer [24]. The **PI** section is the **transitory zone** where the second derivative of the velocity goes from the positive to the negative values. The section that is found downstream of the separation point of the boundary layer is called **wake** [2]. In the wake zone, the flow loses considerably its kinetic energy and the pressure values drop. The dimensions of that wake are **directly influenced by the boundary layer**, which can be laminar or turbulent.

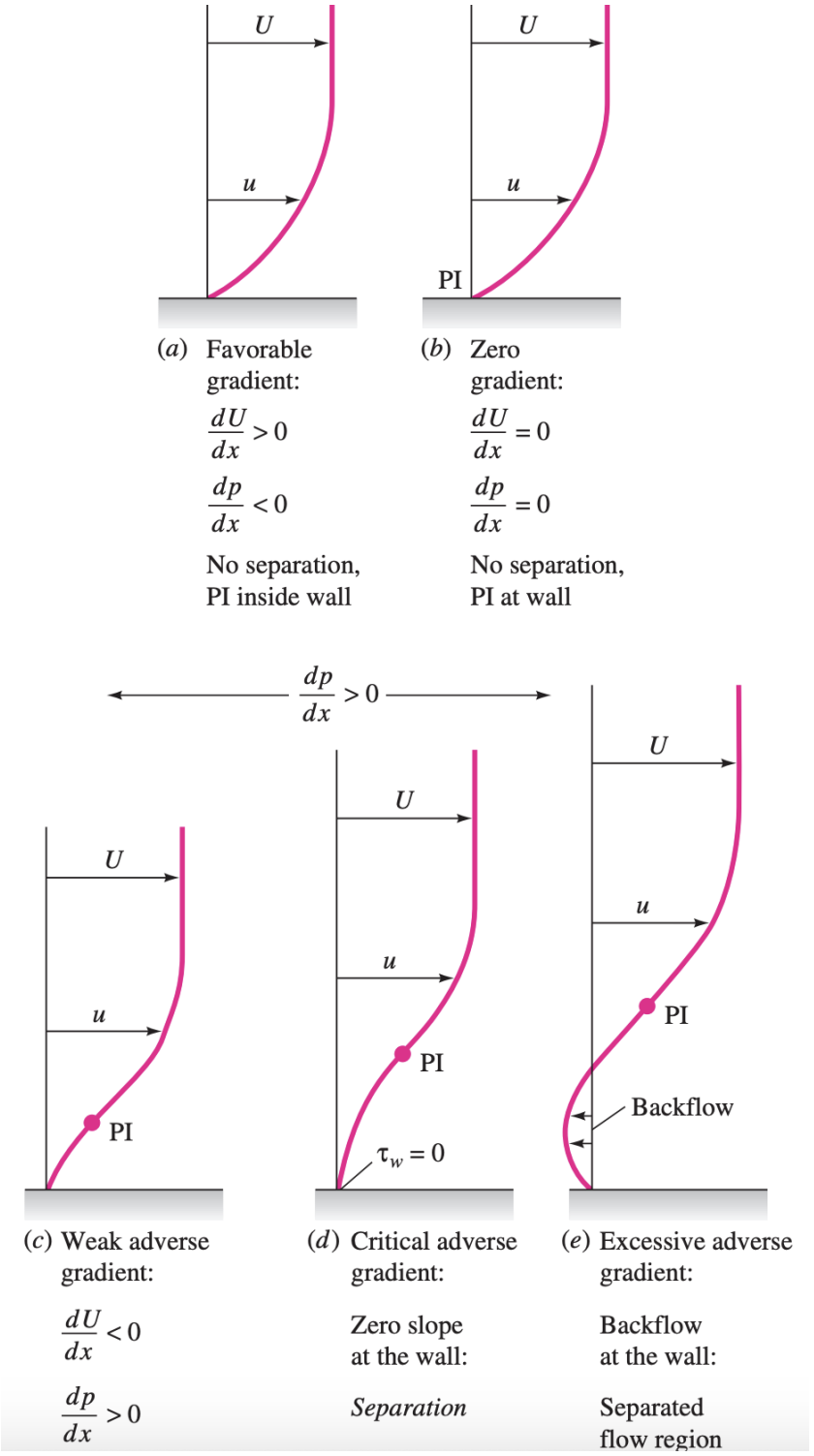

Figure 1.3: Boundary layer separation. Extracted from [2].

1.6 Governing Equations

After having acquired the basic knowledge about Fluid Mechanics, it is time to present the reader the fundamental and **governing equations** that dictate and explain the behaviour of the fluids.

1.6.1 Reynolds Transport Theorem

The Reynolds Transport theorem relates the conversion from a system analysis *SA* to a **control volume** *CV* analysis. A control volume is often described as a specific region in the space that a system may reside in at a given time. A control volume may be **fixed, movable or variable**, as seen in Figure 1.4. This allows that the fundamental equations of fluid mechanics can be also applied to concrete regions instead of doing it to systems of masses.

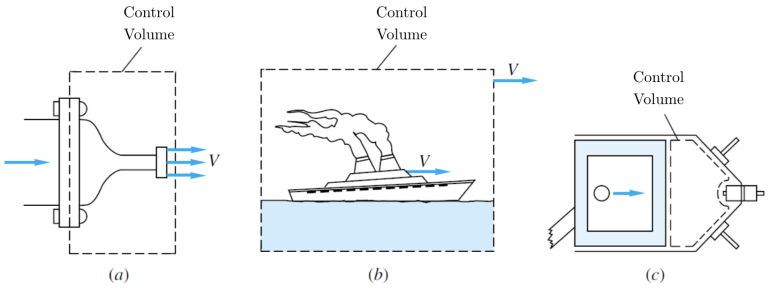

Figure 1.4: Fixed (a), movable (b) and variable (c) control volumes. Extracted from [2].

Considering "K" any physical property of the fluid and κ = dK/dm being the quantity of "K" for every unit of mass in a reduced amount of fluid. The total quantity of "K" enclosed by the control volume (CV) is expressed as:

$$K = \int_{CV} \kappa \cdot \rho dV \tag{1.4}$$

Then, the Reynolds Transport Theorem shown in Equation 1.5 expresses the **temporary variation of K in the system**. The second term refers to the temporal

variation of K within the control volume and the latter one expresses the variation of K by the entrance and exiting of the flow in the CV by means of a control surface CS [2].

$$\frac{\mathrm{d}}{\mathrm{d}t}\left(K_{syst}\right) = \frac{\mathrm{d}}{\mathrm{d}t}\left(\int_{CV} \kappa\rho dV\right) + \int_{CS} \kappa\rho(V \cdot n)dA \tag{1.5}$$

1.6.2 Mass conservation

This principle, also known as the continuity equation simply enunciates that **the rate at which mass enters into a system is the same at which mass abandons the system plus the accumulative term** of mass inside the system [27].

$$\frac{\mathrm{d}m}{\mathrm{d}t} = 0 \tag{1.6}$$

In a differential form:

$$\frac{\partial\rho}{\partial t} + \nabla \cdot (\rho\mathbf{u}) = 0 \tag{1.7}$$

If the flow is considered stationary and incompressible, this yields to:

$$\vec{\nabla} \cdot \vec{u} = 0 \tag{1.8}$$

1.6.3 Momentum Equation

This fluid equation expresses **Newton's Second Law**, that is, that the rate of change in the amount of movement of a given portion of fluid is equal to the resultant of the forces acting on this portion [2]. In other words:

$$\sum \vec{F} = \frac{d(m\vec{u})}{dt} \tag{1.9}$$

So, applying Reynolds' Transport Theorem for a certain CV, it is possible to obtain the integral equation and then, the **differential form** as seen in Equation 1.10:

$$\rho\frac{\partial\vec{u}}{\partial t} = -\rho(\vec{u}\cdot\vec{\nabla})\vec{u} + \vec{f}_T \tag{1.10}$$

The description of the total sum of forces applied can be expressed as **the sum of internal forces** such as the viscosity effects and pressure grandients— and the **external ones** —such as gravitational effects, although the same equation could also contemplate electromagnetic forces and other complex fields— [24]. This way, the resultant equation is:

$$\rho\frac{\partial\vec{u}}{\partial t} = -\rho(\vec{u}\cdot\vec{\nabla})\vec{u} + \rho\vec{g} + \vec{\nabla}\cdot\vec{\vec{\tau}} \tag{1.11}$$

Where $\vec{\vec{\tau}}$ represents the stress tensor.

1.6.4 Navier-Stokes Equations

The biggest problem in the equation above is the **calculation of the stress tensor**. This tensor groups both **normal and tangential stresses** [24]. It is important to note that normal stresses are not those from the pressure, as pressure is not defined from a strict form for fluids with movement (see [28], chapter 3), but it is possible to define an analogous expression for the pressure to the one used in static fluids just as: $p = -\frac{1}{3}\tau_{ii}$

This way, the stress tensor is formed by two parts, the isotropic part and the anisotropic part —with its trace being zero—:

$$\vec{\vec{\tau}} = \underbrace{-p\mathbb{I}}_{\text{isotropic part}} + \underbrace{\vec{\vec{\tau}'}}_{\text{anisotropic part}} = \begin{pmatrix} -p & 0 & 0 \\ 0 & -p & 0 \\ 0 & 0 & -p \end{pmatrix} + \begin{pmatrix} \tau_{xx}+p & \tau_{xy} & \tau_{xz} \\ \tau_{yx} & \tau_{yy}+p & \tau_{yz} \\ \tau_{zx} & \tau_{zy} & \tau_{zz}+p \end{pmatrix} \tag{1.12}$$

It can be shown that, for Newtonian fluids, $\vec{\vec{\tau}'}$ is related to the symmetric part of the velocity divergence by Equation 1.13:

$$\vec{\vec{\tau}}' = 2\mu \left[(\vec{\nabla}\vec{u})^S - \frac{1}{3}(\vec{\nabla}\cdot\vec{u})\mathbb{I} \right] \tag{1.13}$$

Where μ is the dynamic viscosity.

Rearranging terms and substituting in the differential equation of Momentum 1.11:

$$\rho\frac{\partial\vec{u}}{\partial t} = -\rho(\vec{u}\cdot\vec{\nabla})\vec{u} + \rho\vec{g} - \vec{\nabla}p + \vec{\nabla}\cdot\left\{ 2\mu\left[(\vec{\nabla}\vec{u})^S - \frac{1}{3}(\vec{\nabla}\cdot\vec{u})\mathbb{I} \right] \right\} \tag{1.14}$$

Which is usually called the ***Navier-Stokes equation of motion***.

However, in most cases, μ **can be considered to be uniform** as the temperature gradients are considered small enough. This way Equation 1.14 becomes:

$$\rho\frac{\partial\vec{u}}{\partial t} = -\rho(\vec{u}\cdot\vec{\nabla})\vec{u} + \rho\vec{g} - \vec{\nabla}p + \mu\left[\triangle\vec{u} + \frac{1}{3}\vec{\nabla}(\vec{\nabla}\cdot\vec{u}) \right] \tag{1.15}$$

With:

$$\triangle \equiv \vec{\nabla}^2 = \frac{\partial^2}{\partial x^2} + \frac{\partial^2}{\partial y^2} + \frac{\partial^2}{\partial z^2} \tag{1.16}$$

If the flow is **incompressible**,$\nabla\cdot\vec{u} = 0$, and the Navier-Stokes equation remains as:

$$\rho\frac{\partial\vec{u}}{\partial t} + \rho(\vec{u}\cdot\vec{\nabla})\vec{u} = \rho\vec{g} - \vec{\nabla}p + \mu\triangle\vec{u} \tag{1.17}$$

1.7 Aerodynamic Forces

Aerodynamic forces are those exerted on a body by a fluid in which the body is immersed, and they **appear as a result of the relative motion** between the bodies and fluids. Aerodynamic forces arise from two causes [2]:

- The normal force due to **pressure** on the body surface.
- The shear force due to the **viscosity** of the gas, also known as surface friction.

This way, it is common to adapt an axis parallel to the free stream flow and positive downstream and its perpendicular axis pointing upwards as a frame of reference [2]. These aerodynamic forces are commonly resolved into three components.

- **Drag** is the component of the force parallel to the direction of relative movement.
- **Lift** is the component of the force perpendicular to the direction of relative motion.
- **Side Force** is the component perpendicular to the other 2, but no further importance is given as it is considered irrelevant.

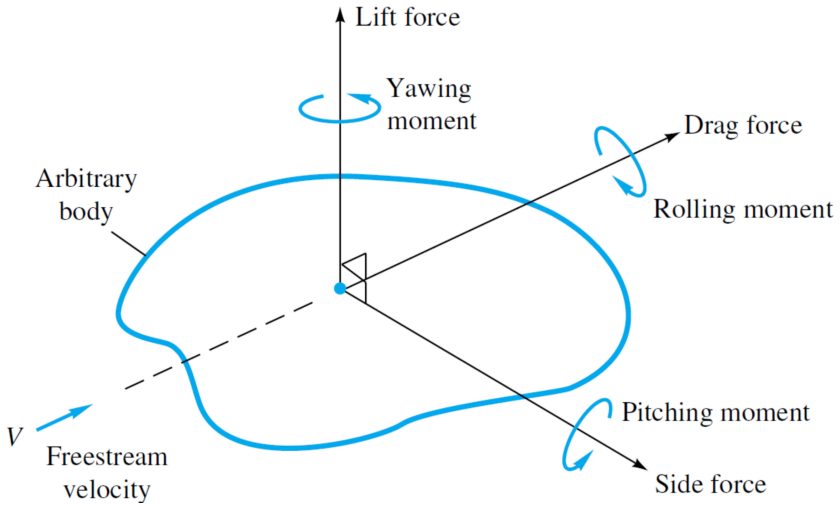

Figure 1.5: Frame of reference of the aerodynamic forces on a body. Extracted from [2].

1.7.1 Drag

As said, Drag is the horizontal component of the aerodynamic forces that **opposes to the movement of the bodies**. It generally produced by two effects:

- The friction forces generated by the fluid on the body creates shear stresses of the boundary layer. Such phenomena is also called **friction drag**.

- The generation of a pressure gradient as a consequence of the difference between the frontal area with respect to the posterior one [29]. At the front, the fluid impacts the solid originating a high pressure region, while at the rear of the body, the boundary layer is separated which develops the wake. This wake is distinguished by being a region of low pressure. The pressure gradient between the two regions generates a force from the highest pressure area to the lowest. This phenomena is called **pressure drag**.

Having stated that, it is common to express the values of Drag force in terms of a **dimensionless coefficient** C_D such that:

$$C_D = \frac{2D}{\rho U_\infty^2 S} \tag{1.18}$$

Where D accounts for the Drag force, U_∞ is the velocity of the flow, ρ is the fluid density and S is the frontal area of the body.

1.7.2 Lift

Again, the Lift force is the one **perpendicular to the speed** of the incident current generated on a body that moves through a fluid. The most common and understandable application is the **airfoil**, a surface generated by an wing profile with a rounded leading edge and a sharp trailing edge as seen in Figure 1.6.

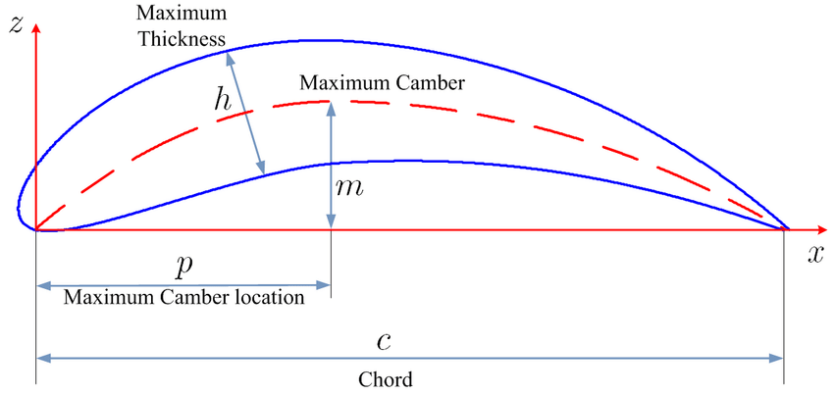

Figure 1.6: Typical airfoil geometry. Courtesy of ResearchGate [3].

There are actually many explanations for the generation of lift, but unfortunately most of them are incorrect and misleading [30]. Lift depends on the shape, the size, the angle, the flow conditions and the **downwash** [1]. The latter is responsible for the generation of an increased velocity on the upper region of the airfoil compared to the lower region. For this reason, as the **Bernoulli's principle** states:

"*An increase in the velocity of any fluid or gas is always accompanied by a decrease in pressure and vice versa*" [32].

This means that the increase of speed in the upper region generates a low pressure zone and the opposite in the lower zone, thus generating lift. Equally, it is common to express the values of Lift force in terms of a **dimensionless coefficient** C_L such that:

$$C_L = \frac{2L}{\rho U_\infty^2 S} \tag{1.19}$$

Some other dimensionless coefficients are the **Efficiency** E defined as the ratio between Lift and Drag:

$$E = \frac{L}{D} = \frac{C_L}{C_D} \tag{1.20}$$

And the **pressure coefficient** C_P, which is normally used to visualise the pressure distribution along the chord of a profile:

$$C_p = \frac{2(p - p_\infty)}{\rho U_\infty^2} \tag{1.21}$$

Where p is the pressure due to the movement of the body through the fluid and p_∞ is the free stream fluid pressure.

[1] Downwash is the change of the air direction due to being deflected by an airfoil [31].

Chapter 2

Formula 1 Aerodynamics

"Aerodynamics are for people who cannot build engines."

- Enzo Ferrari, *Le Mans, 1960.*

The present chapter is aimed at covering the fundamental state of the art **architecture in terms of aerodynamic design of Formula 1 cars** by leading the reader through the path of the history of automobile racing.

Aerodynamic package

The aerodynamic architecture of a Formula 1 car has remained somehow stable since the **introduction of wings** by Colin Chapman in the *Lotus 49B* in 1968 [33] —see Figure 2.1— inspired by other various cars such as the *Chaparral 2F*. This does not mean in any way that aerodynamic development has remained static, in reality it means quite the opposite. The efforts on racing engineering as well as the aeronautical development during the last 50 years have **pushed all those concepts** to the extent as nowadays are conceived. The following sections pretend to navigate with the reader through these well-established and **consolidated aerodynamic concepts**.

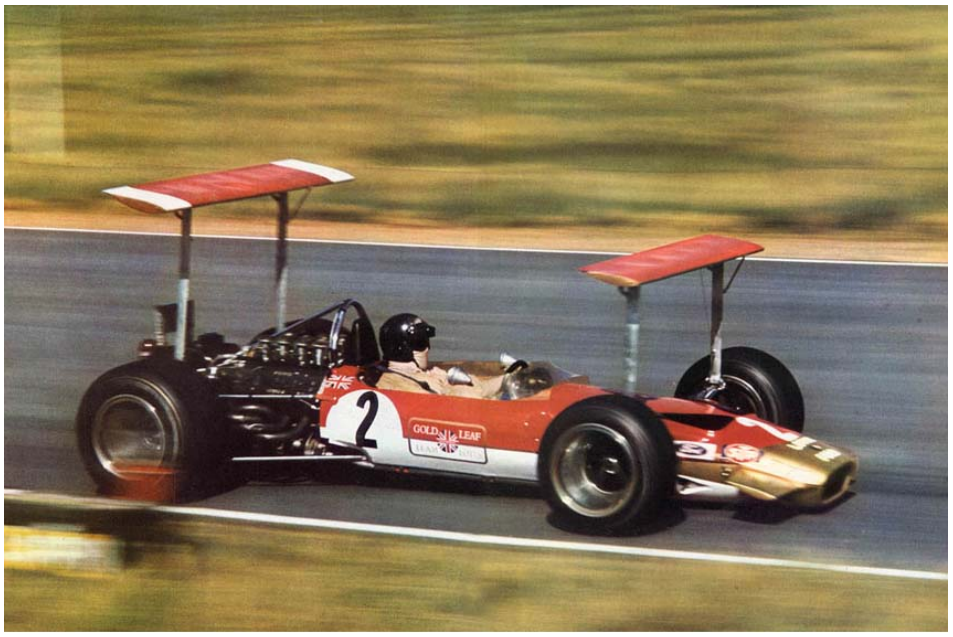

Figure 2.1: Jochen Rindt in the *Lotus 49*, 1969. Extracted from [4].

2.1 Front Wing

The front wing is unarguably **one of the most critical aerodynamic devices** on a racing car. Not only producing the desired front downforce, but also determining the behaviour and quality of flow to the rear parts of the car, notably by attempting to minimise the disturbance created by the front wheels [34].

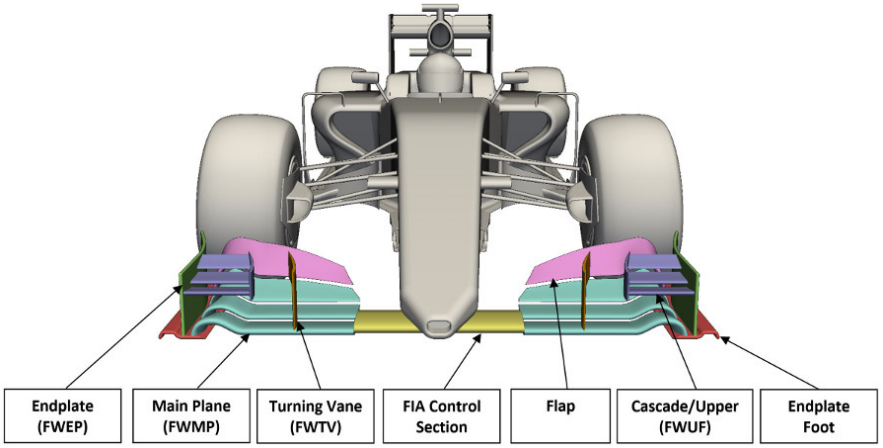

Figure 2.2: Individual components of a current F1 Front Wing. Extracted from [5].

One critical factor that often determines the development of the front wing is the condition in which it operates. It has to be considered that the front wing is **the only important aerodynamic load generating device exposed to the free stream**. This means that a large amount of energy can be obtained from this device, which ends up manifesting itself in both **downforce** and **drag**. In other words, the front wing is aerodynamically very sensitive to small geometric perturbations and as a result, it is extremely complex to operate.

On the other hand, the front wing operates under the **Ground effect**. This physical phenomena is characterised by a **sudden increase of the pressure as the proximity between the ground and the wing decreases**. This occurs at an exponential speed —until the wing stalls—. This effect is responsible for the increase of the overall efficiency and is also the reason why modern tendencies tend to operate the car with an **extreme rake** [34] –low front height and high rear height meaning that the front wing stands closer to the ground–.

Figure 2.3: Front Wing detail of the Williams *FW41*. Extracted from [6].

However, as the front wing is located forward of the front wheel axle line, quite small variations in the height may lead to relatively large changes in proximity

to the ground of the front wing. Therefore, **aerodynamic loads can severely change and end up to sudden variations in whole aerodynamic balance** [5]. This way, another objective of the front wing design is to mitigate the amount of "ride height dependency" in order to design a car with a constant aerodynamic balance —ideal case—. Solving the handling height sensitivity is probably one of the most challenging aspects of a front wing design.

As said earlier, front wings are also responsible for transmitting the flow to the rear of the car in such a particular way that other aerodynamic devices can work more efficiently. At this point, elements such as Endplates and Flaps —see Figure 2.2— play an **important role by being responsible for the generation of tip vortices** as seen in Figure 2.3. The main purpose of the a vortex generator in a front wing is to **disperse the chaotic and turbulent wake that the front tyres produce** so that the flow is redirected away from the operation zones of the diffuser and the rear wing [35]. There are 2 key effects that endplates tend to search in terms of vortex generation: the *outwash* and the *inwash* [36]. In the case of the latter, the airflow is diverted towards the inside of the wheel and rejoins the normal circulation of the flow. A very well-known case is the famous **vortex Y250**, which is called like that because it is created 250mm from the cars' center-line.

However, the **outwash does generate a serious problem** as the airflow is moved from the car through small extensions, causing the generation of a low pressure area around the car. This area of low pressures causes the car behind to be found with *"dirty"* air if it gets too close, **losing aerodynamic load and therefore performance** [36]. That loss of downforce is truly what makes it very difficult to follow and overtake the car in front. Figure 2.4 aims to show some of these vortex generators.

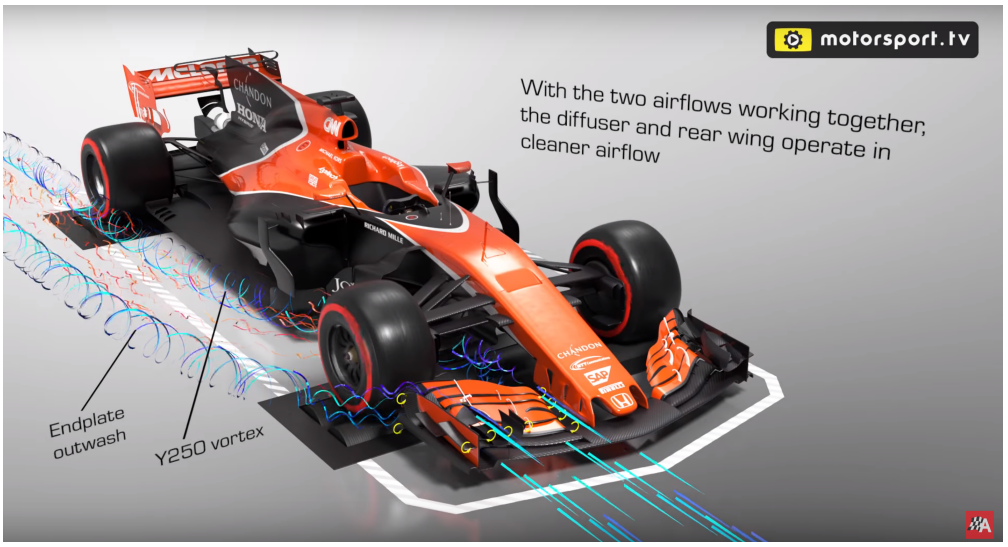

Figure 2.4: Flow around the McLaren *McL32*. The vortex generators disperse the flow far away from the tyres' wake. Courtesy of Autosport [7].

2.2 Tyres

Wheels are the only physical geometry of a F1 car that is actually in direct contact with the ground, and although the tyres' provider is the same for all the teams, the **aerodynamic treatment** of these is always a key point. Several minor controversies such as the holes in the rims that Mercedes starred in 2018 regarding the benefits of suctioning the airflow around the rims to prevent the tyres overheating have been constantly a recent trend.

However, as commented in section 2.1, tyres are one of the biggest headaches in terms of aerodynamic behaviour because of the large, chaotic and **turbulent wake that they despair** over the posterior sections of the car [37]. Formula 1 is mainly characterised by being an open-wheeler series of racing cars thus in terms of aerodynamic performance, wheels produce both lift —which is obviously undesirable as opposed to downforce— and such an amount of drag as they are kept rotating and exposed at high angular velocities. The **wake is the result of the whole flow separation**, as the air flows over the body of the tyre. The wake is distinguished by a region of flow containing several whirls and recirculation

zones. The lowered dynamic and total pressure on the wake mixed with the high pressure in front of the tyres result in a vast pressure drag force [38].

2.3 Bargeboards

Although bargeboards were initially implemented to protect the radiators from dirty air created by the front tires, its main development over the 2000's led to the **complex areas** that can be nowadays seen in modern F1 cars [39]. These elements are curved and vertical planes located longitudinally among the front tyres and the sidepod area. Normally, these elements are significantly higher in the front rather than in the rear, which creates a trapezoidal shape curved outward in plan view. Also, they are closer to the center line of the car in the front and they tend to bend towards the rear, see Figure 2.5.

Aerodynamically, **bargeboards act as flow redirectors** ensuring that turbulent air from the front wing, the front suspension links and the spinning front wheels is guided away from the aerodynamic surfaces downstream. This means that the lower region of the bargeboards causes several vortices that travel around the car acting as a skirt, **helping to seal a low pressure area under the car**. These deflectors are also used to reduce the speed of direct air inlet to the sidepod —and therefore, the speed with which the air reaches the radiators and the engine area— reducing, in turn, the drag that they generate in the sidepods [40].

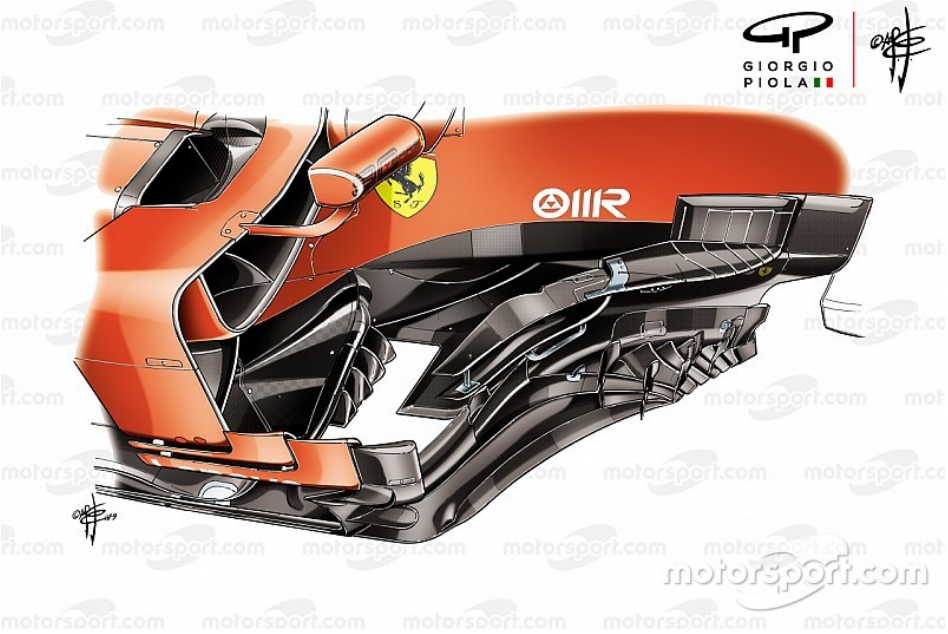

Figure 2.5: Detail on the Ferrari *SF90* Bargeboard zone. Courtesy of Giorgio Piola [8].

On the other hand, bargeboards are typically accompanied by an element called turning vane which is located further forward, between the front wheels and the monocoque. This devices are so-called because they are designed fundamentally to turn the airflow around the car. The turning vanes are responsible for multiple functions, but are **utilised predominantly to ensure the control of the turbulent wake from the front tyres** and to scavenge the airflow from the front wing and the under-car area, turning the airflow towards the sidepods, the floor and the diffuser.

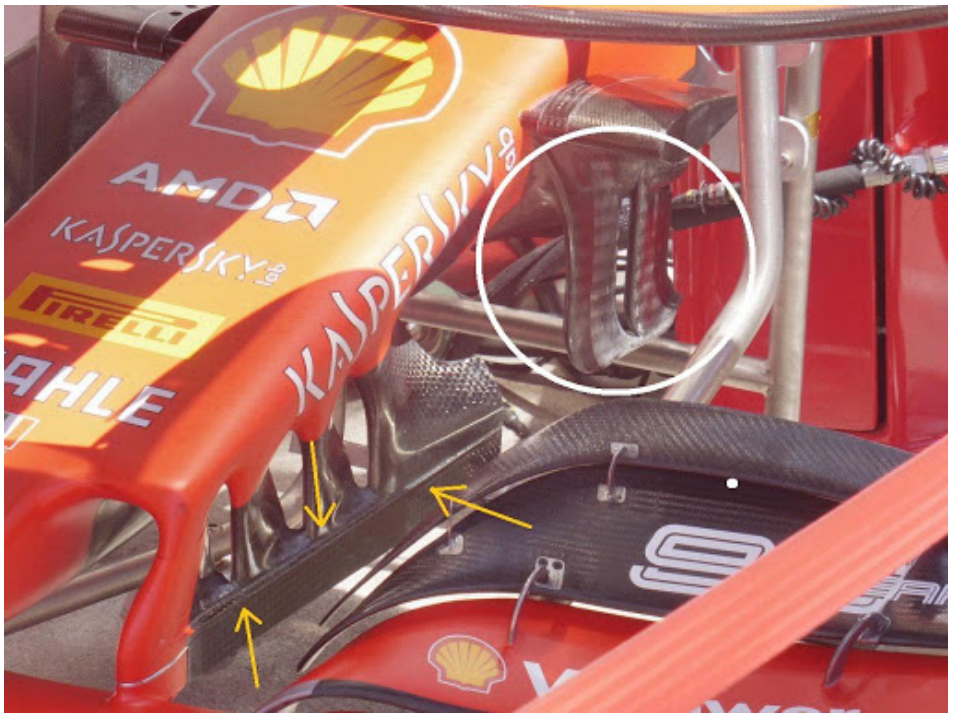

Figure 2.6: Ferrari *SF90* turning vane for the Austrian GP. Courtesy of F1 Analisi Tecnica [9].

2.4 Sidepods

Despite being refrigeration the main goal of the sidepod area, this peculiar region has become **one of the most well-developed sections on F1 cars** in recent times. As said, sidepods tend to be as slim as possible in order to minimize the drag caused by the big and exposed open section of their entrance, so that there is **a compromise between the cooling and the aerodynamic performance** [41]. See Figure 2.7.

Figure 2.7: Detail of the Mercedes *W09* sidepod area for the Monaco GP. Courtesy of Motorsport.com [10].

However, the sidepod area is also responsible for **canalising the flow of the rear part of the car**, which is indeed, where the biggest downforce generation occurs. These elements prevent air from going straightforward to the rear tire because thanks to its shape, the airflow that would initially affect the tire is directly sent away to avoid undesired turbulence. The usage of **vortex generators** in the upper surface of the pods is very common to obtain these attachment effects. The other key part is of course, the flow redirection to the lower sections of the car such as the floor as it is a rather energetic section in terms of resources. It should be noted that the air sticks to the surface of the sidepod —where the engine cover is placed—, thanks to the **Coanda effect** [32]. This effect can be summed up as the ability or tendency of a fluid to remain attached to a surface whether the shape of the latter allows it. As mentioned in Chapter 1, (see section 1.7.2), the **Bernoulli's principle** rules that behaviour, which is perfectly shown in equation 2.1 and Figure 2.8.

$$P_1 + \frac{1}{2} \cdot \rho_1 \cdot v_1^2 + \rho_1 \cdot g \cdot h_1 = P_2 + \frac{1}{2} \cdot \rho_2 \cdot v_2^2 + \rho_2 \cdot g \cdot h_2 \tag{2.1}$$

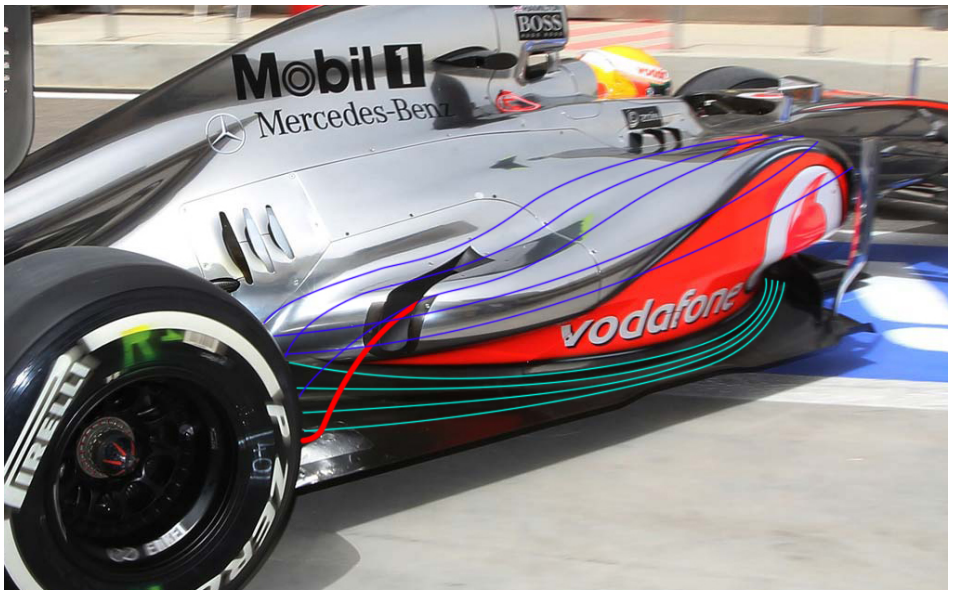

Figure 2.8: An example of how the Coanda effect works on the McLaren *Mp4 26*. Extracted from [10].

It is important to recall the above **stated compromise** between the merging of the sidepods with the surfaces that accompany them in order to design the car **as slim as possible without generating cooling problems**. This was a quite unusual trouble for McLaren during the 2015 season as they introduced the concept of *Size 0* that led to a very narrowing of the back of the *MP4 30* as the Honda Power Unit was said to be smaller than their rivals. This, which initially was seen as a very valuable drag reduction ended up being the main source of cooling problems, overheating and of course, a decrease on performance.

2.5 Floor

This section has been with no hesitation one of the most developed and rather interesting parts of F1 cars for more than 40 years.

As a product of Colin Chapman's importation of knowledge to the Lotus team, **Ground effect technology dominated the aerodynamic development** in F1 from the late 70's to the 80's, leading to impressive benefits in terms of cornering speed and overall downforce gains. The fundamentals of ground effect were

based on exporting an aerodynamic principle known as **Venturi effect**, where the underside of the car was designed in order to make the whole chassis act like **one huge wing which sucked the car into the ground** [11]. The *Lotus 79* was presented as the innovation on what was possible by modelling the underside of the sidepods and sealing in the low pressure by means of side skirts, see Figure 2.9. However, it is rather interesting to note that ground effect was accidentally discovered and not intentionally designed when the Lotus team tried to attach their car in their wind tunnel and found impressive downforce levels. This point caused the start of the **sealed skirts innovation** race among all the teams.

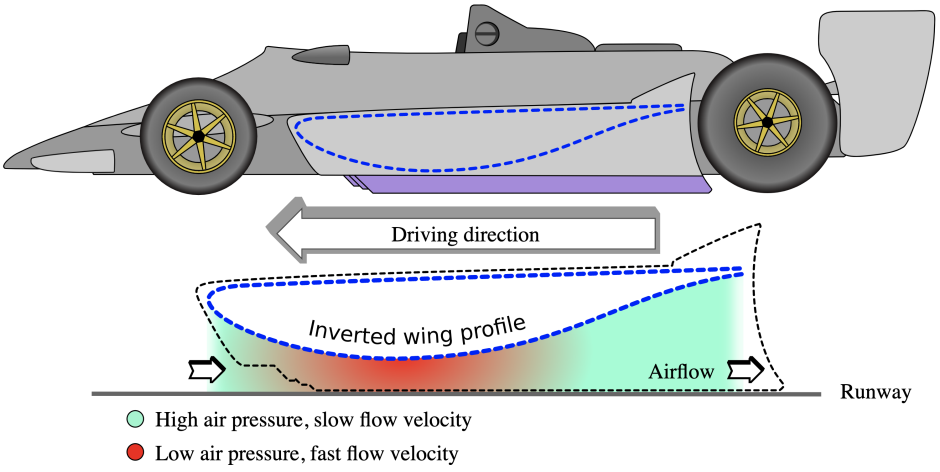

Figure 2.9: Lotus *79* Ground effect design. Extracted from [11].

As one of the main —if not the biggest— advantage of the Ground effect principle is the **high Lift to Drag ratio**, unlike the addition of wings on the upper surface. This means that the whole aerodynamic package was conceived to generate the vast majority of the downforce from the lower part of the car and seal it with skirts.

On the other hand, drastic and extreme concepts adopting the ground effect principles were presented such as the case of the Brahbam *BT 46* which was renamed as the fan car, see Figure 2.10. The vehicle designed by Gordon Murray was said to have critical cooling problems as the Alfa Romeo V12 engine was too wide to be able to imitate the sidepod area of the Lotus *79*, which was the key to perform properly under the Ground effect. This way, the car incorporated a **massive fan**

on the rear part of the car and alleged the FIA [1] that the fan was installed to help with the cooling problems and not with aerodynamic purposes.

However, the fan generated a huge suction area that, with the help of the skirts was sealed and helped the car achieve vast levels of downforce impossible to be equalised without this device. The innovative solution was banned after its first race due to several controversies involving the impossibility to follow the fan car due to the big amount of dust and debri that it generated.

Although theoretical principles seemed good enough —and indeed they proved to be in the windtunnel— in reality the Ground effect cars proved highly unpredictable as they **were not able to guarantee a constant level of downforce** and huge losses of it appeared when the skirts suffered from damage or were partially removed. This caused that in 1983, after a campaign blighted by a number of serious accidents, Ground effect technology was banned. In its replace, **mandatory flat floors** between the inside tangent of the tyres and no-skirts models were fixed by ruling, and their dimensions, fixed [42].

Figure 2.10: Brabham *BT 46* named as the fan car. It was able to generate a high-suction area under the floor which was sealed with skirts. Extracted from [12].

[1] Federation Internationale de l'Automobile

Modern Formula 1 cars have their underside heavily regulated. The floors have a regulated design called step plane, so only a small area, behind the rear axle is now allowed to become an expansion area [43]. So, basically there are **3 key elements to create Ground effect** in the modern aerodynamic rules: Bargeboards, the diffuser, and the suspension. This combination altogether helps to create front forward rake on the cars, as seen in section 2.1 that leads to create a pseudo widening in the flat floor which helps to achieve an expansion area as seen in Figure 2.11.

Figure 2.11: Detail of the Ferrari *F10* (left) and the Mercedes *W09* (right) floors. Extracted from [13].

2.6 Diffuser

The diffuser is the aerodynamic part of the car that is **responsible for generating the most amount of downforce** —approximately around 50 % of the total downforce— from the underside of a F1 car. The airflow that moves under the car as mentioned in section 2.5, exits through the diffuser, which is located by the rules, behind the rear axle line [44].

Despite working similarly, wings and diffusers are based under different approaches in terms of design. The **diffuser is used to eject the air out from the underside of the car**. This fact causes that the velocity of the air under the car increases, so that the slower moving air above the car creates a **suction effect**

on the car that sticks it to the ground. This effect is a natural consequence of Bernoulli's principle —already stated in 2.4—, therefore the pressure under the race car must be lower than the pressure found at the outlet since the velocity of the airflow under the car will be higher than the one at the outlet. Figure 2.12 is aimed at showing this physical principle.

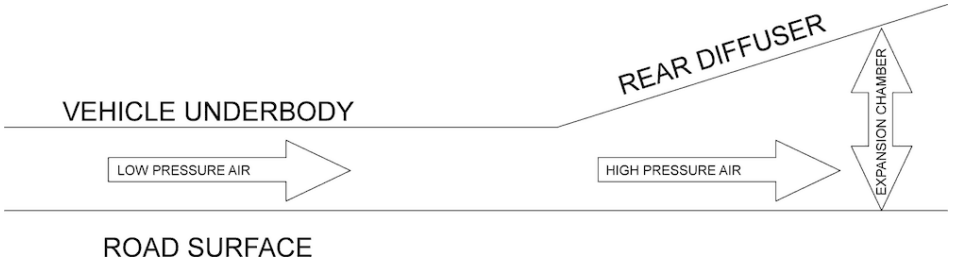

Figure 2.12: Simplified drawing of a diffuser functioning.

It is important to note that the diffuser itself does not produce a reduction in the pressure values. The role of the diffuser is based on **expanding the flow from underneath the car to the rear**, which at the same time reduces the flow's velocity from inlet of the diffuser to the outlet. This pressure's potential, accelerates the flow underneath the car resulting in reduced pressure and as such, an increase of downforce generation. This **difference of pressure is a function of the ratio of the surfaces** from the inlet and the outlet of the diffuser, where such area ratio is established by the diffuser angle and the car ride height [45].

It is very important to ensure that the diffuser is carefully shaped to avoid no separation of airflow which might really reduce the effectiveness of the overall floor. This way, **vertical strakes** are usually found in diffusers as their function is to keep apart and seal the many different types of airflows found at the back of the car [46]. All these various types of airflows have different energy levels and different speeds, and their separation makes them easier to deal with. Strakes are also **vortex generators**, but they are far more complex and definitely harder to design for this approach. This is basically because the vortex generated is required to be in the base tunnel of the diffuser to improve its performance [46]. Turbulent regimes underneath the floor can also damage the performance as pockets of higher pressure —which may upset the stability of the car's underbody— can be created.

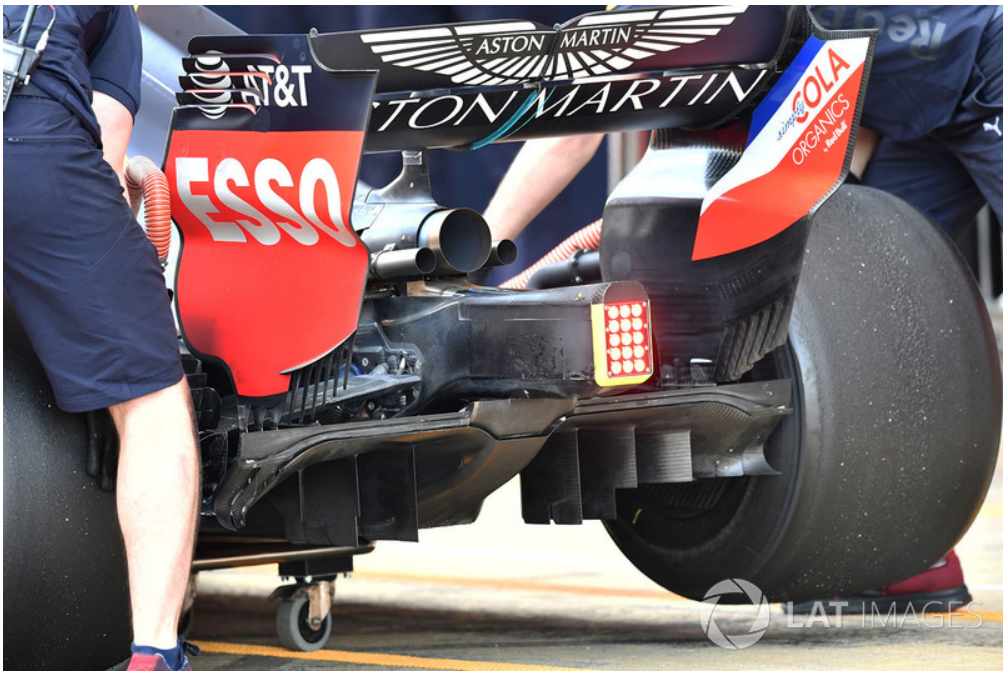

Figure 2.13: Detail of the RedBull *RB14* diffuser. Courtesy of Motorsport.com [14].

One of the biggest controversies of the recent times regarding the usage of diffusers occurred at the beginning of the 2009 season, following the new regulation change. **Brawn GP** —a team that was built from the scratches of the old Honda Racing F1 Team— unveiled its tittle contender for the 2009 season with very competitive preseason testing laptimes. The car, wich was actually orphan of any sponsors, turned out to lead the aerodynamic revolution of the field by using a **revolutionary concept in its diffuser**. The new regulations intended to cut down the downforce of the cars by reducing the size of the diffuser and thus, improve the overtaking. However, a loophole was left open that allowed the **placement of a second diffuser** into the crash structure that was fed by two holes in the floor of the car [47]. This controversial area allowed Brawn GP —as well as Williams and Toyota in a similar way— to open up a very large and significant entrance that allowed them to **expand the airflow much sooner** than a conventional diffuser [18].

Despite the protests and demands from all other teams, the FIA declared the double-decker diffuser tweak as legal and eventually it led to Brawn GP **winning both** the drivers and the constructors championships that year.

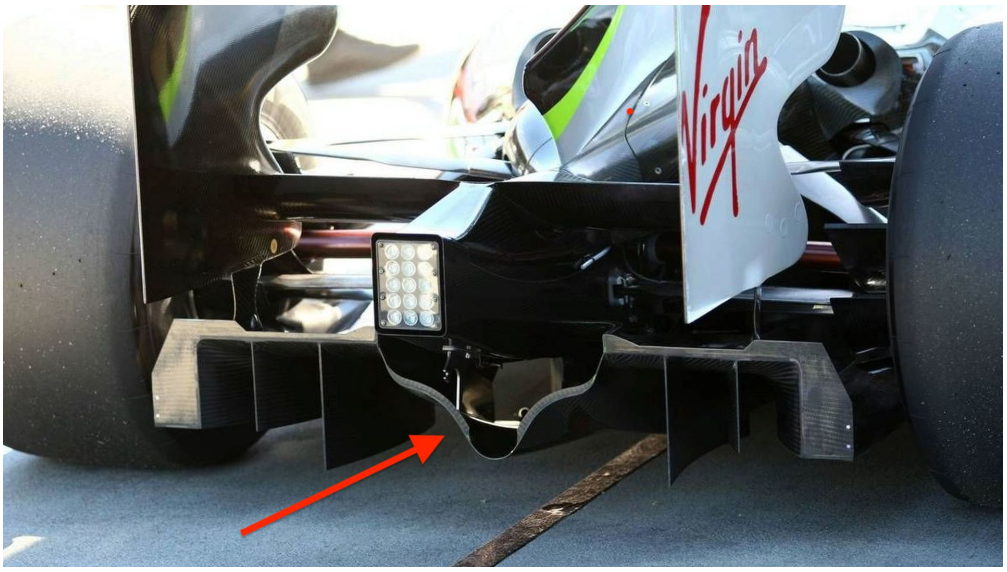

Figure 2.14: Detail of the Brawn *BGP 001* double diffuser. Extracted from [15].

2.7 Rear Wing

Finally, if the reader has successfully managed to follow and understand the basics of F1 aerodynamics, the rear wing functioning should not be a cause of trouble.

The rear wing of a F1 car works as a **conventional airplane wing**, but instead of demanding a generation of lift, rear wings are designed upside down in order to **generate a certain amount of downforce** [48]. A wing profile is characterised by having a certain curvature on the upper surface that ranges from the leading edge *LE* to the trailing edge *TE*. If it is assumed that two neighbouring fluid particles which diverge at *LE* experience a downwash effect until the *TE*, then this requires a certain velocity difference between both surfaces. This way, Bernoulli's principle again 2.1 enunciates that that increase in the velocity is accompanied by a decrease in pressure thus, the lower surface will generate a force pointed upwards the upper surface [49]. So keeping that knowledge in mind, as said earlier in 2, rear wings were introduced in the late 60's into F1 with only one purpose in mind: **generate downforce** on the rear of the car. However, the natural evolution of the wing concepts led to the primary introduction of the so-caleed **endplates located at the tips of wings** that intend to reduce the **vortices** generated by

the wing and in turn, create more downforce. According to Hoerner [50], endplates increase the effective wing aspect ratio AR thus, increasing the contribution in the parabolic curves of the lift coefficient as seen in Figure 2.15.

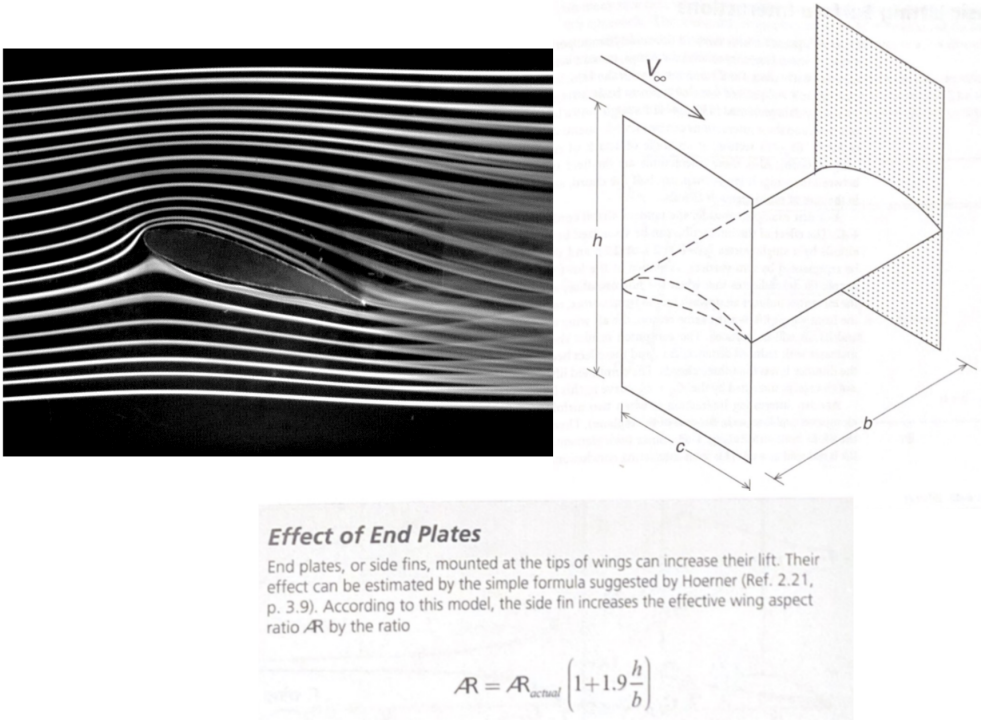

Figure 2.15: Flow around a wing and detail on the endplates contribution. Extracted from [16].

As opposed to the diffuser and the underside elements of a F1 car, rear wings generate as well a **big amount of drag** as the frontal area of these elements tends to be quite large. This is why, the introduction of the *DRS*, **Drag Reduction System** in 2011 aimed at trying to facilitate the overtaking maneuver. The system itself minimises the drag generated by the rear wing as the main flap is opened and the frontal surface is reduced. This device is only available to be used within a straight line as its opening while in a turn causes an undesired dynamic balance thus, causing the driver to lose control of the car.

Finally, as mentioned before, the generation of big vortices in the rear wing is a totally **undesired phenomena** as it is related with induced drag. As it is obvious, after the rear wing there are no more upcoming surfaces to redirect that

airflow so, a constant drag generation on the rear part would only upset the overall performance of the car.

Figure 2.16: Wingtip vortices on the rear of the McLaren *Mp4 26*. Extracted from [17].

Chapter 3

Tools of the trade

"The last thing one discovers in composing a work is what to put first."

- Blaise Pascal, *Pensées, 1670.*

This chapter intends to illustrate the reader about the modern and most used techniques to study and test the aerodynamic concepts of F1 cars: **CFD techniques**, **Wind Tunnel testing** and **Track Testing**. However, the latter 2 will not be covered as a special emphasis will be placed in the CFD techniques due to being the main tool concerning the evaluation of the present study.

CFD Techniques

Computational Fluid Dynamics (*CFD*) is the branch of the Fluid Mechanics that uses **numerical methods** and algorithms in order to solve and analyse the behaviour of the fluids. In order to use CFD techniques, it is quite important to know as much as possible about the real problem that is intended to be simulated —this are the physical properties of the fluid, the boundary conditions of the problem as well as other variables—. After that, a compendium of mathematical equations are the fundamental tool needed to solve the problem. These equations are indeed, the **Navier-Stokes equations** [51] as presented earlier in 1.6.4.

However, the difficulty of these equations **resides in their inherent non-linearity** [51], which requires the usage of different control volumes to rewrite the equations into an algebraic form and solve them numerically.

3.1 Numerical Methods

As said, Numerical Methods are mathematical techniques to solve numerical problems. The procedure consists of **obtaining algebraic equations** starting from differential equations in order to obtain approximated solutions by means of discretized domains. Currently there are several numerical methods available to use in CFD, but as *OpenFoam* solvers used in this study use **FVM**, the explanation will be focused on this method.

3.1.1 Finite Volume Method

"The Finite Volume Method is a discretization technique that is well suited for the numerical simulation of different types of **conservation laws**. This method is locally conservative as it is based on a **balance approach**: A local balance is written on each discretization cell that is called Control Volume." [1]

These Control Volumess **contain nodes** that are organised with a reference frame that takes into consideration their neighboring nodes. The main node is designed as P and the adjacent nodes are named after the cardinal points as N (North), S (South), E (East) and W (West).
On the other hand, the contiguous faces to the main node are also determined equally as n, s, e and w as seen in Figure 3.1. After that, the **conservation laws are derived for each cell** so it is feasible to determine iteratively the fluid properties distribution throughout the field of study [53].

[1] R Eymard, T Gallouët, R Herbin. Finite Volume Method [52].

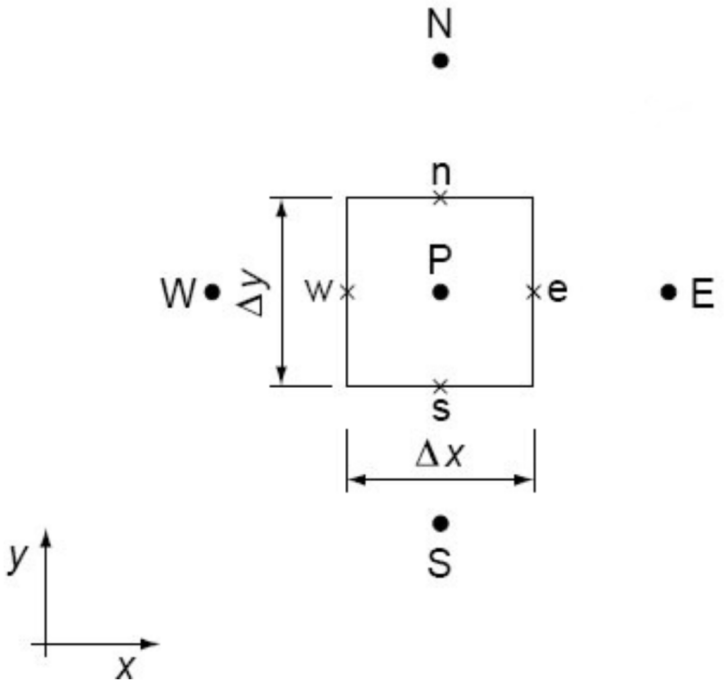

Figure 3.1: FVM Discretization. Extracted from [18].

3.2 Pre-processing

It is usually considered that Pre-processing tasks take a **time contribution of around 70%** of the total time estimated to run a case. This includes both the Geometry preparation, and the meshing process.

3.2.1 Geometry preparation

One of the key points of a CFD simulation is based on the quality of the geometry. This means that the **CAD model should be specifically prepared for the CFD process**, and this includes its the simplification or adaptation without establishing a big compromise with the original problem.

Typical examples include the **merging** of surfaces, the **smoothing** of certain edged or steep areas, and the direct **suppression** of controversial elements that would hinder the meshing process.

3.2.1.1 Flow Domain

Sometimes it is also important to include the whole flow domain as part of the geometry instead of generating it by means of a mesh. A fluid domain is the **finite region for which the fluid circulates**. This domain adopts internally the shape of the desired object to be studied and its size depends strictly on the specific case studied. However, it is important to note that if the geometry is **symmetric**, it is rather advisable to carry out the simulation only in one half of the geometry. This will significantly reduce the quantity of elements to be studied, thus **reducing computational resources** and time.

3.2.2 Mesh

Once the final volume of the study is properly defined, the next natural step is to mesh it in order to be able to solve the Navier-Stokes equations on different **small Control Volumes**, as seen in 3.1.1.

This is again one of the key points on a simulation, as an excessively coarse mesh will potentially affect the accuracy of the results.

The most common types of mesh can be divided into **3 different categories**: Structured, unstructured and mixed.

- **Structured mesh**: Regular connectivity that can be expressed by a 2D or 3D array of numbers [54], as seen in Figure 3.2.

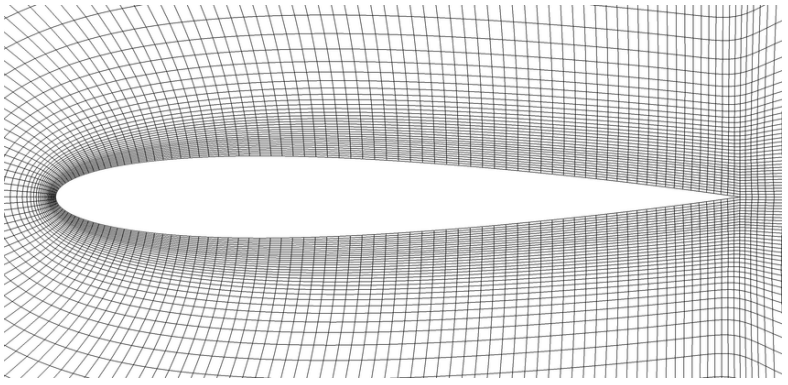

Figure 3.2: Example of structured mesh. Extracted from [19].

- **Unstructured mesh**: Complex connectivity [54]. It is usually used in complex geometries due to its good adaptation. See Figure 3.3.

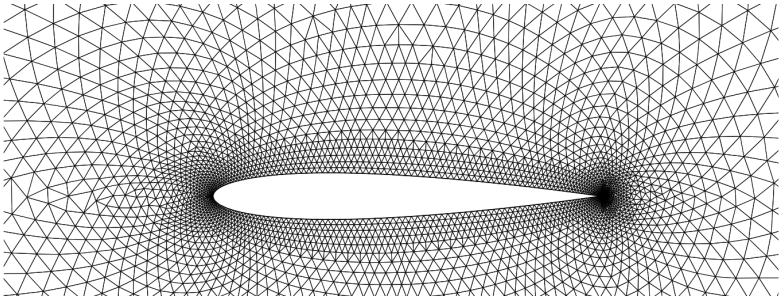

Figure 3.3: Example of unstructured mesh. Extracted from [20].

- **Hybrid mesh**: Uses a combination of the latter 2. That enables the creation of the most suitable mesh depending on the area of the geometry studied. See Figure 3.4.

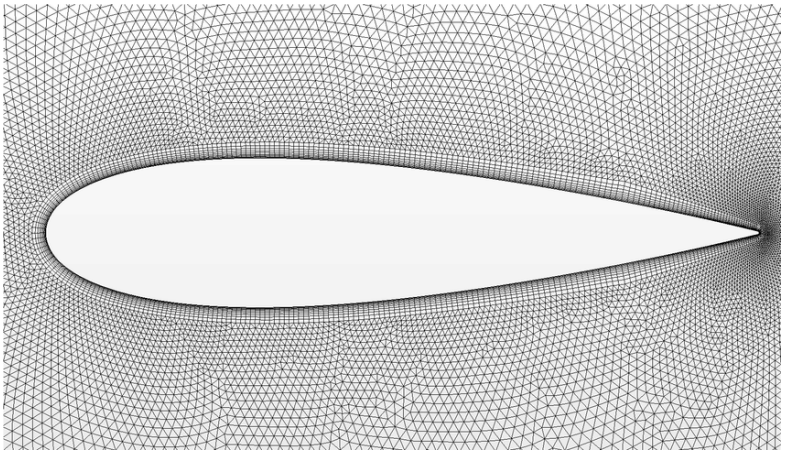

Figure 3.4: Example of hybrid mesh. Extracted from [21]

.

3.2.3 Quality of the mesh

In order to discern whether the quality of the mesh is **sufficient enough** or not, it is important to check a series of parameters. The quality of the mesh is essential to determine whether the solution is independent of the mesh and to capture properly the geometrical details [55]. The general quality criteria are:

- **Aspect Ratio**: It is defined as the ratio of cell sizes in different dimensions. This number should be kept as close to 1 as possible.
- **Orthogonality**: Measures the angle between the imaginary line that connects two cell centres and the perpendicular of their common face. Numbers above 75° are considered to require a special treatment such as *nonOrthoCorrectors*. Above 90° indicates a bad mesh, which cannot be used to simulate.
- **Skewness**: Measures the degree of sameness between the real element and the ideal described by the one circumscribed inside a sphere. Numbers below 30 are considered acceptable [56].

3.3 Processing

After having successfully achieved a proper mesh generation, the next step is to set up the simulation. This includes the definition of the **boundary conditions** —which are given by every particular problem—, the **fluid properties**, the **solver used**, the **turbulence models**, etc. It is usually stated that this stage takes around 10 % of the total time.

For this reason it is extremely advisable to acquire a sufficient amount of knowledge about the models available in order to be able to **discern the most optimum option** for a certain problem. When talking about turbulence, it is important to note that the usage of models comes from the necessity of being unable to solve the **non-linear convective term** [57] in the Navier-Stokes equations (See 1.6.4).

The most common turbulence models are [58]:

3.3.1 RANS

It is based on decomposing the variables of the problem into **an average value and a fluctuating one** to model the Reynolds tensor than comes from the convective term [57]. It is possible then to rewrite the equations with the averaged variables, but to close these system of equations, there are several models that can be used:

- **K - ε**: A quite common model used for its **robustness** and **low computational cost** under incompressible flows with high *Re* number. Two extra equations are required: The dissipation rate of energy ε and the transport of energy K.

- **K - ω**: Rather similar to the latter but the model is **less linear** as this includes the solution of the specific rate of dissipation of kinetic energy ω.

- **SST**: This model **combines the latter 2**. It uses K - ε along the free stream flows while in the near wall section uses K - ω.

- **Spalart-Allmaras**: Composed of one single equation and it is usually used within **aerodynamic purposes** — e.g., flows around airfoils—. It is stable and offers a good convergence, but sometimes the **flow separation causes issues** to it [18].

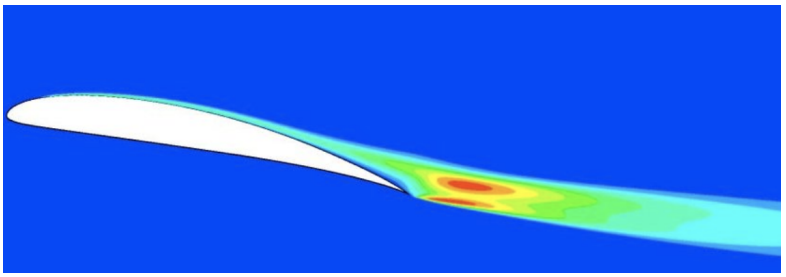

Figure 3.5: RANS simulation of an airfoil. Extracted from [22]

.

3.3.2 LES

It focuses on the concept of **filtering rather than averaging**. Usually offers better results than RANS models [57], but the computational resources required are much bigger. It is very accurate for turbulent flows in transition regimes but the mesh is required to be a way finer, specially near the wall.

3.3.3 DNS

In fact, it is **not a model** as it is based on directly solving the Navier-Stokes equations without any turbulence model. For high *Re* numbers in complex geometries, it is still beyond the available computer resources.

Near Wall Treatment

It is of extreme importance to bare in mind that the boundary layer treatments always require a **special attention**. As it is not always possible that the first cell from the wall is placed within the viscous sub-layer, the usage of **wall functions** becomes more relevant [23]. For this reason, the $y+$ parameter is introduced as a dimensionless number that defines the distance between the first node and the wall. Specific values of this parameter are recommended depending on the type of wall function. See equation 3.1.

$$y^+ = \frac{y \cdot u_t}{v} \tag{3.1}$$

$$u_t = \sqrt{\frac{\tau_{\text{turb}}}{\rho}} \tag{3.2}$$

$$\tau_{\text{turb}} = \frac{1}{2}\rho \cdot U^2 \cdot C_f \tag{3.3}$$

Where y is the distance between the node and the wall, v is the kinematic viscosity, τ_{turb} is the wall shear stress, ρ is the density, U is the velocity and C_f represents the coefficient of friction.

The different zones of the turbulent boundary layer according to their $y+$ value can be designated as:

- **Viscoussub-layer**: $(y+ < 5)$
- **Transition layer**: $(5 < y+ < 30)$

- **Logarithmic-layer**: ($y+ > 30$)

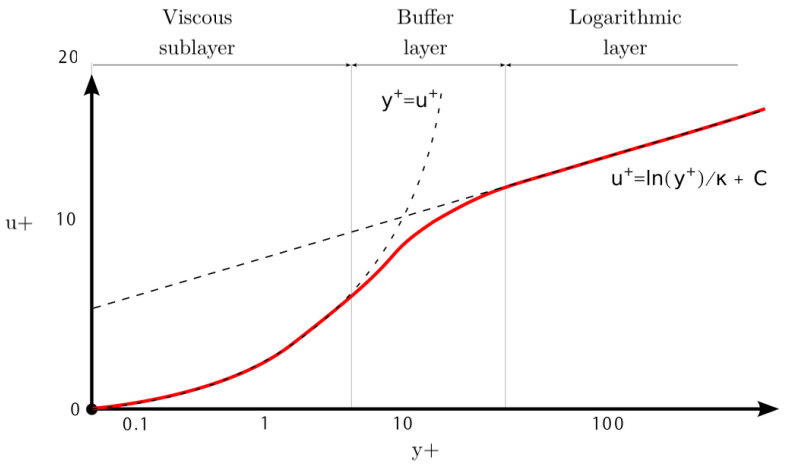

Figure 3.6: Boundary Layer zones. Extracted from [23].

3.4 Post-processing

Having already performed the simulation process, it is necessary to **evaluate the obtained results**. This includes the variables of interests, the required calculations, plots, extraction of data, comparisons, etc. It is considered that this stage consumes around 20% of the total time.

Part II

Approach

Chapter 4

Problem Statement

> *"Sir, I am a modest man, and I would settle for you to pay me a grain of wheat for the first square of the chessboard, two for the second, four in the third, and so on."*
>
> - Sissa Ben Dahir, *Possible origins of chess, AD VI.*

The present chapter is aimed at trying to evaluate the **most feasible way to develop the problem** stated initially in this study. As earlier mentioned in the objective, the purpose of the present study is based on the quantification of the aerodynamic forces on a 2017 spec. adapted F1 car by means of CFD techniques.

Available resources and justification of the chosen solution

Two feasible and effective solutions were initially evaluated for the development of this work.

The first one is the usage of ***OpenFoam***, which involves the acquirement of the basic knowledge of this *C++* library as well as a remarkably powerful source of computational power.

On the other hand, the alternative was based on the usage of the ***Simscale*** plattform, which is directly fed by an *OpenFoam* core. This plattform disposes of a graphical interface that makes the learning curve a bit less steep, although it still requires a certain background knowledge of CFD. However, the main advantage that this option offers is the huge capacity of **computational power** with an "*Academic Plan*".

After having evaluated both alternatives, it was initially thought that *OpenFoam* could offer a more challenging approach to the project. For this reason, **several tests were performed** in a 6-core i7 machine with 16Gb of RAM in a Linux distribution with *OpenFoam* installed.

After a couple of months of tutorials, testing and until a considerably good knowledge of *OpenFoam* was reached, it was regrettably seen that the computational power required to perform this project was **beyond the limit**. The cases evaluated regarding the F1 geometry were considerably coarse —less than 1 million of cells— and the models proposed were kept very simple —e.g: no rotational speed in the wheels—. As a result, the computational time was around 12 hours for the meshing process and around 8 hours for the simulation. This meant that a quite unrealistic model of a very coarse mesh would take 20 hours to generate some results that, in the end, **proved to be not representative at all** of the real solution.

For this reason, it was believed that the present study would potentially require an amount of computational resources that were not available physically. The personal **compromise** with the achievement of **realistic results** at the cost of sacrificing the tool that had been so useful to learn about CFD **prevailed**.

After that, the reevaluation of the *Simscale* plattform was considered by means of a pros and cons table —see Table 4.1—. As it is possible to check, *Simscale* not only offers the same amount of advantages as *OpenFoam*, but also **overcomes drastically the latter** in terms of pure power, memory capacity and physical dependency although it is restricted to an internet connection and a maximum computational core hours of 3000.

On the other hand, as a good background of CFD was previously achieved with *OpenFoam*, it was believed that all that **knowledge would be quite essential**

and reusable with *Simscale*, which would ease the learning curve.

For all the above stated reasons, the resource designated to perform the CFD simulations is the ***Simscale*** plattform. However, **by no means** it is intended to state that **Simscale is better than OpenFoam**, only that under the particular circumstances of this study it offers more advantages than drawbacks.

	OpenFoam	Simscale
Nº of cores available	6	32
RAM memory (Gb)	16	64
Physical machine required	Yes	No
Knowledge required	Yes	Yes, but already acquired
Energy consuming	Yes	No
Specific and direct support	No	Yes
Usage of open-source solvers	Yes	Yes
Internet connection required	No	Yes
Computational core hours	Unlimited	3000

Table 4.1: Main features of each evaluated option.

Part III

Development of the problem

Chapter 5

Free Stream condition

"Rules are for the obedience of fools and interpretations of smart men."

- Colin Chapman, *CAR interview, 1968.*

As presented earlier, the first scenario of the study consists of the analysis of a **F1 car under a free stream scenario**. This means, that the model is simulated alone, with no interference nor perturbation.

5.1 Geometry preparation

As mentioned earlier in 3.2.1, it is essential to obtain a proper geometry that is sufficiently representative of the real problem without severely compromising the simulation process.

The F1 car developed by PERRIN [59] —an engineering community with experience in F1— was **modeled according to the 2017 FIA regulations**. For this reason, it was considered that this particular geometry was the **most suitable and accurate representation** of a contemporary F1 car. Figure 5.1 shows the geometry used.

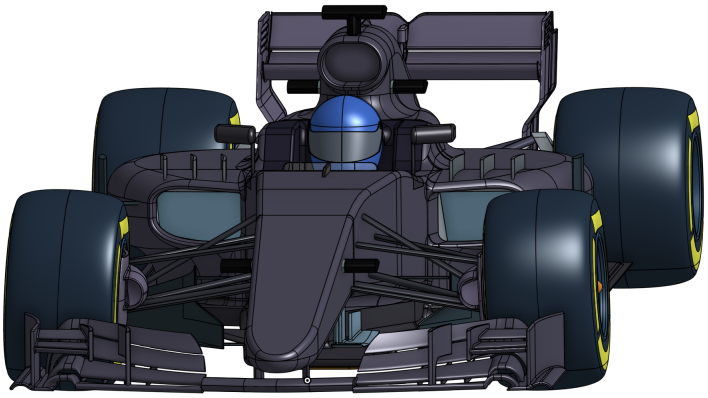

Figure 5.1: Isometric view of the F1 car CAD model.

The preparation process includes the **clean up and fixing** of the most common topology defects, such as overlapping edges and surface cracks. As this is a very complex model —composed by 117 solids and around 5510 faces—, the correction tasks were harsh and complicated. However, a particular focus was placed on several critical zones of the model, whose quality determines the success of the mesh: wing strakes, turning vanes and suspension arms, etc. For this reason, smoothing features were added to **avoid skewness and non-orthogonality** problems.

On the other hand, it is important to mention that a **general merging** of the elements was **intended** —creation of group entities that would reduce the number of elements and surfaces— as seen in [60]. However, due to the complexity and creation process of the geometry, the merging tools from Onshape, SolidWorks and Salome —Boolean operations— **did not allow** to obtain a simplified agrupation of entities. This somehow hinders the post-process of the simulation as the selection of elements becomes harder and convoluted, but does not harm the meshing nor the simulation. This way, it was decided to carry on with proposed geometry.

It is also important to note that a fluid domain, whose dimensions are specified in 5.3, is also included as part of the geometry to avoid future problems with the meshing.

Last but not least, the geometry was exported in ***Parasolid*** format (*.x_t.*) so as to be processed by the *SnappyHexMesh*. This format was preferred to other options such as *STL* since the quality of the it is directly influenced by the quality of the volume mesh and hence the **accuracy of the results**.

5.2 Simulation Resources

As mentioned earlier in Chapter 4, The *Simscale Academic plan* disposes of a machine equipped with **32 cores and 64Gb of RAM memory**. The post-processing operations were carried out by means of an i7 six core laptop with 16Gb of RAM.

5.3 Mesh

First of all, it is important to comment that the **fluid domain length** is set as the one proposed by [59]. The reference length L is set as **5.3 m**, which corresponds to the length of the car.

Besides, as the geometry is symmetrical and the simulation is steady, **only one half** of the vehicle is considered for the simulation. This way, the total domain length is 13.5 times the vehicle length. The downstream section occupies 8 car lengths and the upstream zone is around 4.5 car lengths. As for the vertical and depth of the domain, both longitudes are fixed at 3 times the car's length so as to be able **to capture properly the wake effects and the generation of vortices**. Figure 5.2 shows the proposed bounding domain.

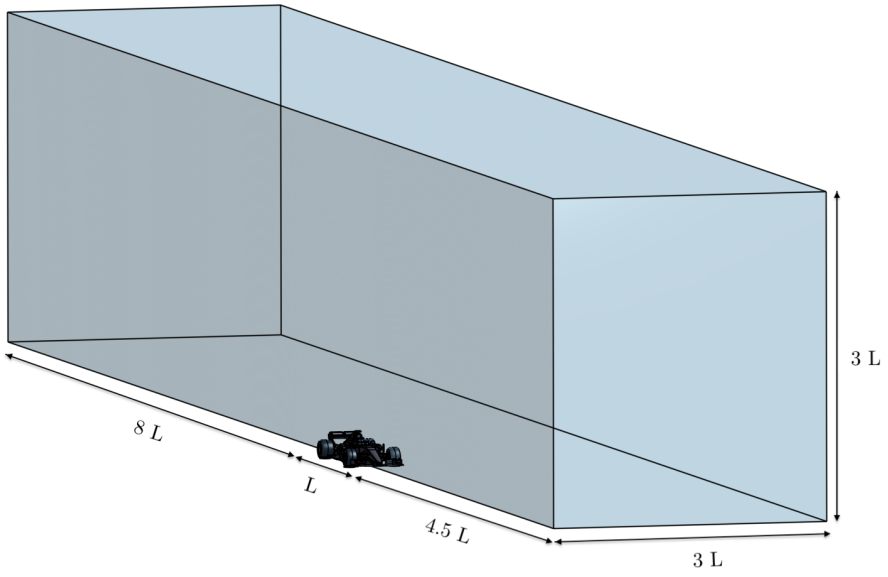

Figure 5.2: Fluid domain dimensions.

As for the mesh, the **main traits** of it can be summed up as follows:

Two different mesh structures were evaluated; a tetrahedral and an hexahedral one (See Appendix A for the discussion). The height of the first cell at the solid surfaces is set at 0.01 mm with a **layer expansion ratio** of 1.3. The resulting average value of **y+** (See 3.3.3) is around **40**, which involves the usage of **wall functions**. In order to be able to capture the effects of the wake and and other phenomena, many **refinement enclosures** were specified along the geometry. A special attention was placed in the massive wake region as well as on the downforce generation zones such as the wings and the floor.
Having achieved all these tasks, the *CheckMesh* command was run locally to detect any skewness problems, aspect ratio defects or non-orthogonality issues. No major problems were found and the **mesh quality was declared successful**. The results can be checked in Figures 5.3 and 5.4.

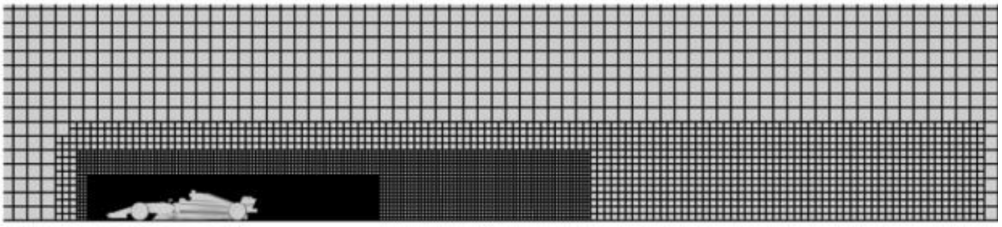

Figure 5.3: Overall mesh and refinement enclosures.

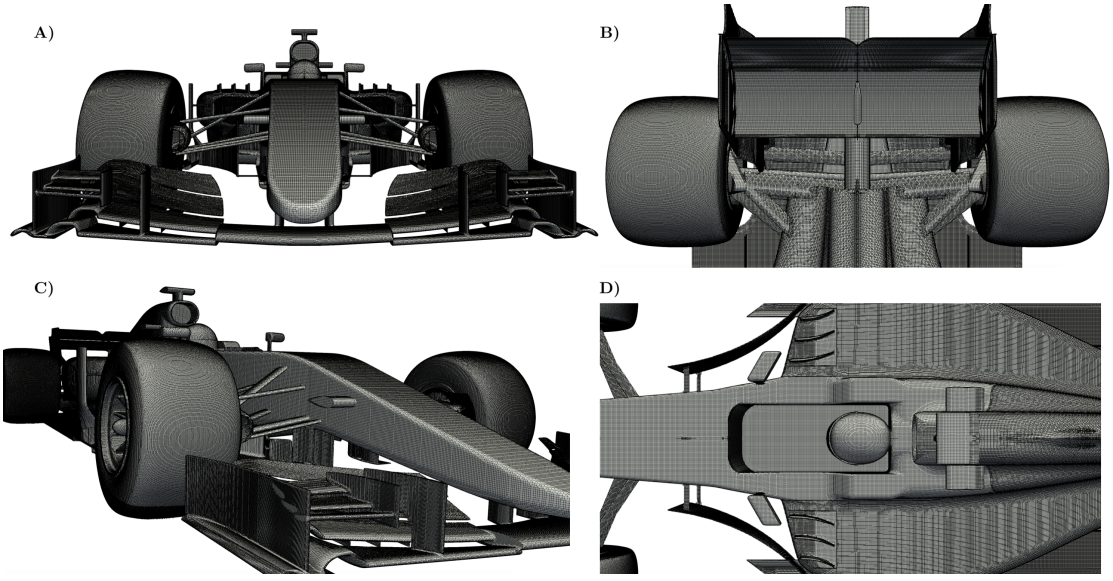

Figure 5.4: Mesh A) Front, B) Rear wing, C) Trimetric, D) Cockpit.

Finally, it is essential to note that a **Grid Convergence Index** (GCI) was performed in order to be able to guarantee that the analysis of the results obtained is **independent of the mesh**. The GCI methodology is performed according to the one proposed by Celik, 2008 [61] and the study is performed by varying the level of definition of the 3 different meshes studied —this is reflected in the **snappyHexMesh** file—. The refinement levels used range from 5–6 in the coarsest, 6–7 in the intermediate and 7–8 in the finest. The ϕ value analysed corresponds to the lift coefficient multiplied by the surface ($S \cdot C_L$). The results obtained of the GCI are presented in Table 5.1.

	$\phi = \mathbf{S}{\cdot}C_L$
N1, N2, N3	18055055, 13793013, 10634551
r_{21}	1.309
r_{32}	1.297
ϕ_1	-3.43
ϕ_2	-3.40
ϕ_3	-3.28
p	4.37
GCI_{fine}	**1.1** %
GCI_{coarse}	**3.7** %

Table 5.1: Grid Convergence Index result of the meshes studied.

As shown in Table 5.1, GCI values are in the **asymptotic range of convergence**, both GCI_{fine} and GCI_{coarse}. It is as well possible to note that the difference in ϕ values between the finest and intermediate meshes is considerably small thus, obtaining a **very small percentage of error**. As for the computational resources, the finest mesh —which is formed by 19.2M cells— took an approximated time of 8 hours to be generated. So, as computational resources do not suppose a huge compromise nor restriction it is preferred to choose the finest mesh for the following study. The **sacrifice** in computational time and consumption is **notably overcome** by the superior amount of **detail and definition** that the finest mesh may deliver.

5.4 Boundary conditions and Setup

The general boundary conditions established are as follows:

- **Inlet velocity** set at 50 m/s
- **Pressure outlet** set at Atmospheric pressure
- **Symmetry plane**
- **Ground velocity** set at 50 m/s
- **Slip condition** on the side wall and the top of the wind tunnel
- **Angular velocity** and rotational axis of the wheels (MRF)

As for the turbulence model, the **k-ωSST is selected** as k-ϵ is used in the outer region of and outside of the boundary layer and k-ω is used in the inner boundary layer. According to [62], it is possible to assign the car wheelbase —representing the size of the largest eddy—, as turbulent length scale l. All these data are shown in Table 5.2.

Finally, the incompressible RANS simulations were executed by means of the **simpleFoam algorithm**. The pressure equation was solved with the **GAMG** solver while **smoothSolver** was used in the velocity and turbulent variables (See Appendix C.1 and C.2). It was considered to reach convergence when pressure and velocity residuals were lower than 10^{-3} and the aerodynamic variables remained stable.

Variable	Value
Free stream velocity U_∞	50 m/s
Fluid density (ρ)	1.225 kg/m^3
Turbulent Intensity (I) [63]	0.15 %
Turbulent length scale (l)	3.475 m
Reynolds Number (Re)	12 $\cdot 10^6$

Table 5.2: Setup of the simulation.

5.5 Results

Aerodynamic performance

First of all, regarding the preliminary comparison between the results obtained, these are **compared with the reference data** proposed by Perrin [64]. The numerical prediction deals with the **aerodynamic coefficients**: Downforce (SC_L), Drag (SC_D), overall aerodynamic efficiency E (C_L/C_D) and Front Balance FB, which is defined as the fraction between the downforce generated by the front axle and the total one.

Table 5.3 shows that the results of the performed RANS simulation with k-ωSST model **encounter a notable agreement** with the reference data [1]. The error found in both downforce and drag coefficient **differs by 4.45 % and 6.50 %** respectively. This indicates that the overall **simulation is successful**, as the difference between the aerodynamic coefficients is found to be small enough to **accept them and validate** the reference datum.

	SC_L (m^2)	SC_D (m^2)	$\lvert C_L/C_D \rvert$	FB (%)
Reference Data [64]	-3.59	1.23	2.92	44.80
Simulation Results	**-3.43**	**1.15**	**2.98**	**41.23**
Error (%)	4.45	6.50	2.15	7.97

Table 5.3: Comparison between the simulation and the reference data.

On the other hand, it is found appropriate as well as interesting to indicate the **relative contribution** in terms of downforce and drag of the main components of the car. This way, it is possible the see the **influence of each element** and appreciate their aerodynamic efficiency —which is very useful in terms of redesign purposes and issues detection—. Figures 5.5 and 5.6 show the distribution of these aerodynamic forces.

[1] Reference data are obtained through a CFD simulation with TotalSim.

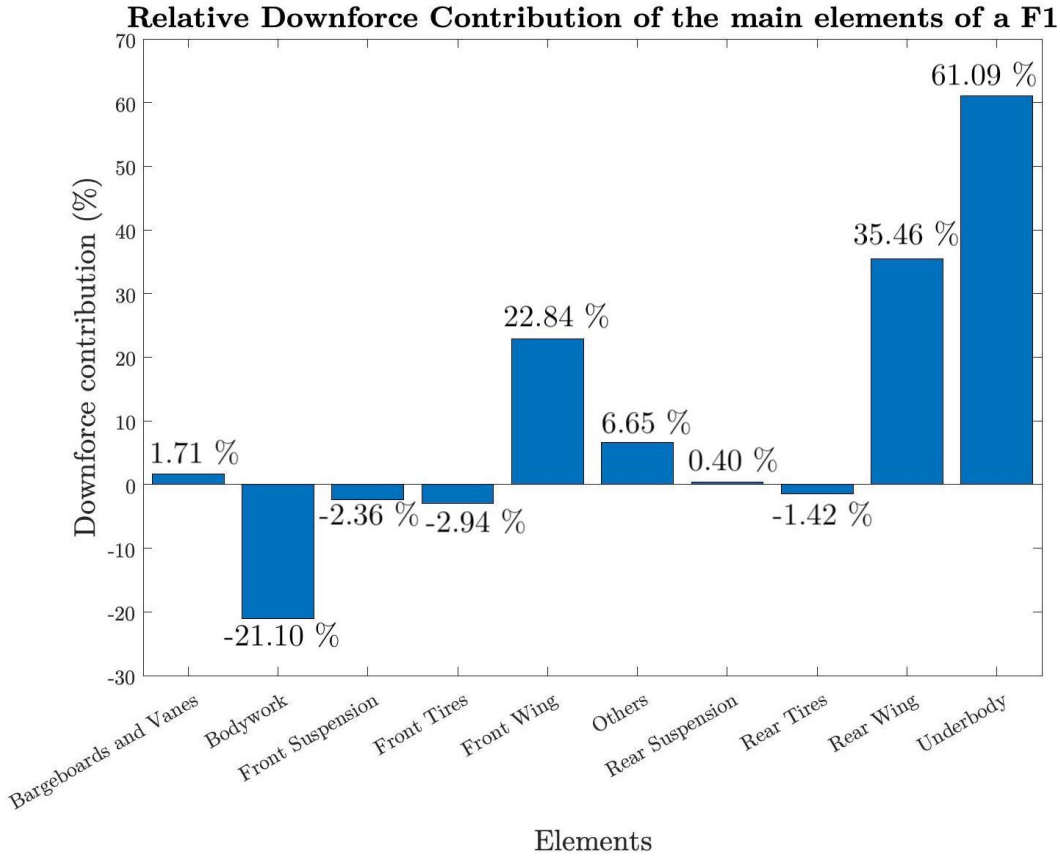

Figure 5.5: Relative downforce contribution.

Some important comments in reference to that matter can be made:

The **underbody** —composed by the flat floor, the plank and the diffuser— is **responsible for the 60%** of the total downforce generation. Following this trend, the **rear and the front wing** represent respectively around **35% and 23 %** of the overall downforce of the car. The **bodywork**, shaped as a wing profile, counterbalances these gains by producing **lift** as well as other elements such as the **front suspension**, and both rear and front **tires**.

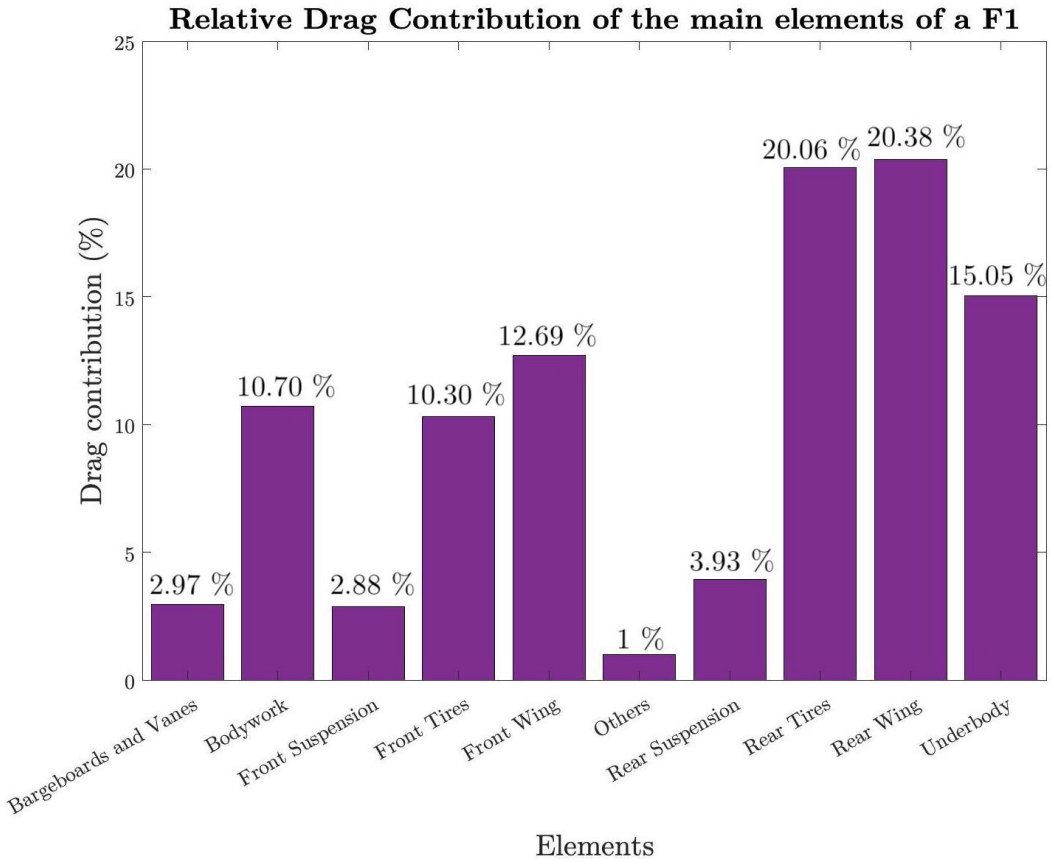

Figure 5.6: Relative drag contribution.

On the other hand, Figure 5.6 shows that **tires** represent around **30% of the total drag** of the car. Also, the **front and the rear wing** are as well present by being responsible of the **13 % and 20 %** of the total drag respectively. Other elements such as the **underbody** (15 % of the drag) and the **bodywork** (10.70%) take an important contribution regarding the aerodynamic resistance.

In terms of aerodynamic efficiency, it is important to note that the **underbody** is with no hesitation **the most efficient part** of the car. This can be explained due to the usage of Ground effect —despite being limited by the flat floor and the size of the diffuser—. As opposed to that, the **rear wing** is known for its low aspect ratio [2], which helps generate **big downforce** quantities, but suffers from the production of **induced drag**. The efficiency of the front wing is somewhere between the underbody and the rear wing: the beneficial points of the rake and

[2]The aspect ratio of a wing is the ratio of its span to its mean chord [65].

ground effect (see 2.1) are counterbalanced by the high angle of attack of the flaps and the vortices generated at the tips.

Finally, the **tires** are responsible for huge quantities of **drag**, specially on the rear tyres, as the wheels are not covered. This area is well influenced and dominated by **big pressure losses** in the wake, which leads to these undesired **high turbulent** zones.

Pressure distribution

Figures 5.7 and 5.8 show the **pressure distribution** by means of the dimensionless coefficient (C_P) around the car. The upper view reflects **high-pressure zones** located in the nose —specially in the front wing— as well the rear wing due to its high curvature. Some stagnation areas are also found around the cockpit, where the pressure distribution is low and smooth. These results go in line with what it was previously commented in 5.5, being the **wings one of the main generators of downforce** due to its high angle of attack and curvature.

On the other hand, the underbody of the car shows **low-pressure zones** under the wings —as it was clearly expected by its nature and shape—. Besides, the low-pressure zones along the **floor and diffuser** suggest that the car is **working properly under the Ground effect**. It is possible to see a smooth transition from a medium pressure zone to a low pressure region —meaning that the airflow is being accelerated— and finally an increase of pressure that returns the airflow in a lower velocity to the wake. However, the region in close proximity to the tires is affected by an increase of pressure, which implies the loss of the Ground effect benefits.

In general, the pressure distribution is rather **smooth** around the car, with **no abrupt pressure gradients nor unexpected transitions**. It can be stated then, that the distribution obtained goes in line with what it is considered a **good behaviour** and an expected result.

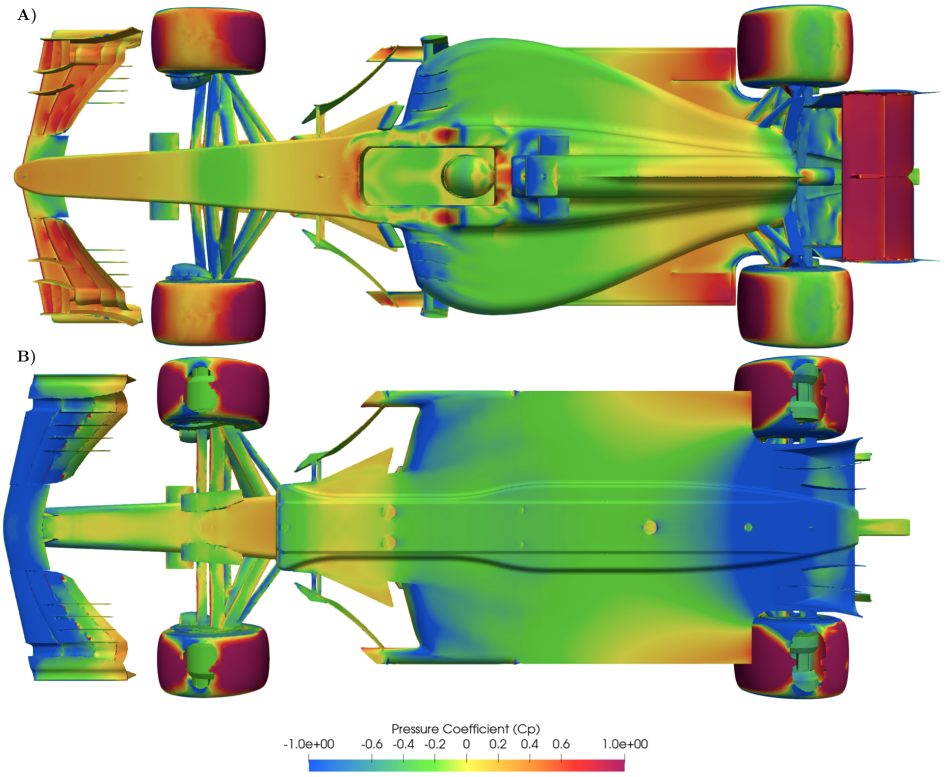

Figure 5.7: Pressure coefficient on the A) Top and B) Bottom views of the car.

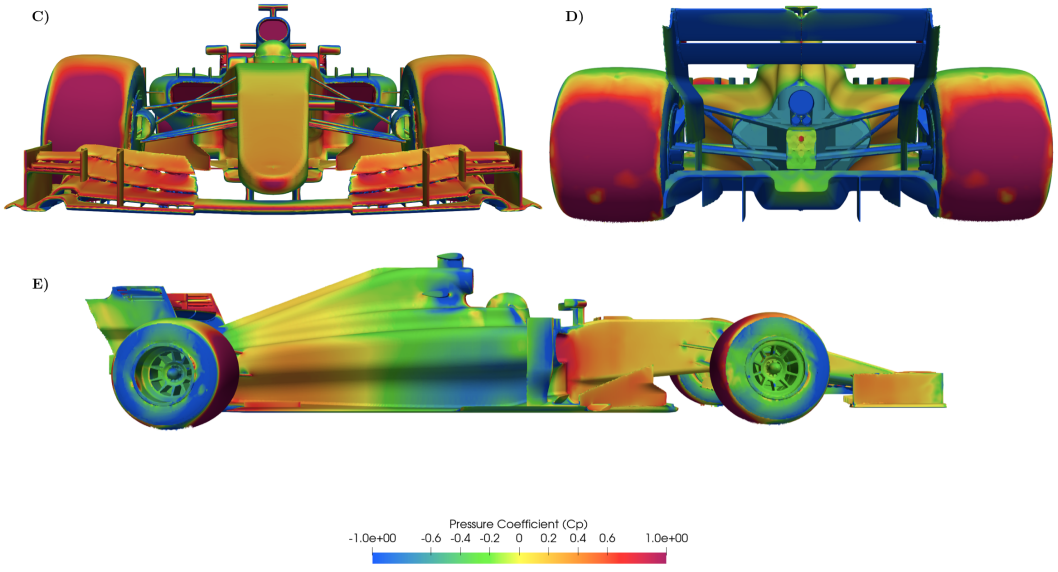

Figure 5.8: Pressure coefficient on the C) Front, D) Rear and E) Lateral views of the car.

Vorticity

The following plots pretend to illustrate the reader about the shape, position and prolongation of some **three-dimensional vortical structures** as well as to provide several details about the strength and the rotational axis of such vortices.

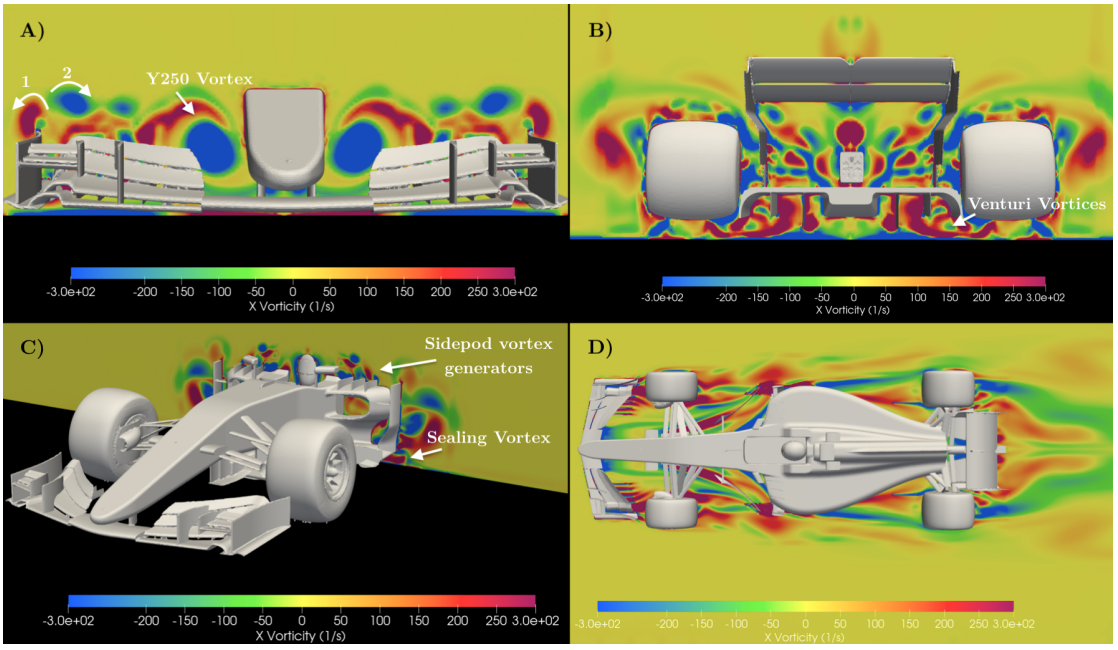

Figure 5.9: Several axial vorticity planes.

Figure 5.9 A) shows the multifaceted front wing: not only generating downforce but also axial vorticity that tends to **avoid the front tires and energises the flow downstream**. Several vortical structures can be seen on the **tip of the endplate** (A1) or the **winglet endplate** (A2), among others. The rotation of the vortices —clockwise or counter clocksiwse— depends on the pressure field around them [66]. A quite interesting phenomena —as it is clearly the biggest vortex generated in the front wing— is the so-called **Y250 vortex**, which was already presented in section 2.1. This vortex is developed between the middle section of the wing and the multi flap surface and is aimed at recirculating the flow towards the underbody of the car (inwash).

As opposed to that, Figure 5.9 B) shows the rear part of the car, where several vortices are originated as a result of the wake of the spinning wheels and other devices. Special attention is placed in the **Venturi vortices** generated on the side of the diffuser due to the pressure gradient between the underbody and the outside. Also the strakes of the diffuser generate small vortices, that are coupled with an opossite rotating vortex due to the interaction with the **ground boundary layer**.

On the other hand, Figure 5.9 C) reflects the generation of **vortices in the upper middle region** of the car. The bargeboards and the vanes play a special and important role here. The goal of the latter is to **seal and canalise** the flow over the bodywork, making sure that the flow keeps attached along the car (see Coanda effect in 2.4). Besides, the sealing vortices generated by the bargeboards tend to act as **skirts**, therefore preventing the underbody airflow to scape and maximise the maximum the Ground effect and the **diffuser efficiency**.

Moving down, Figure 5.9 D) displays a top view of the car to understand the behaviour of the overall vorticity.

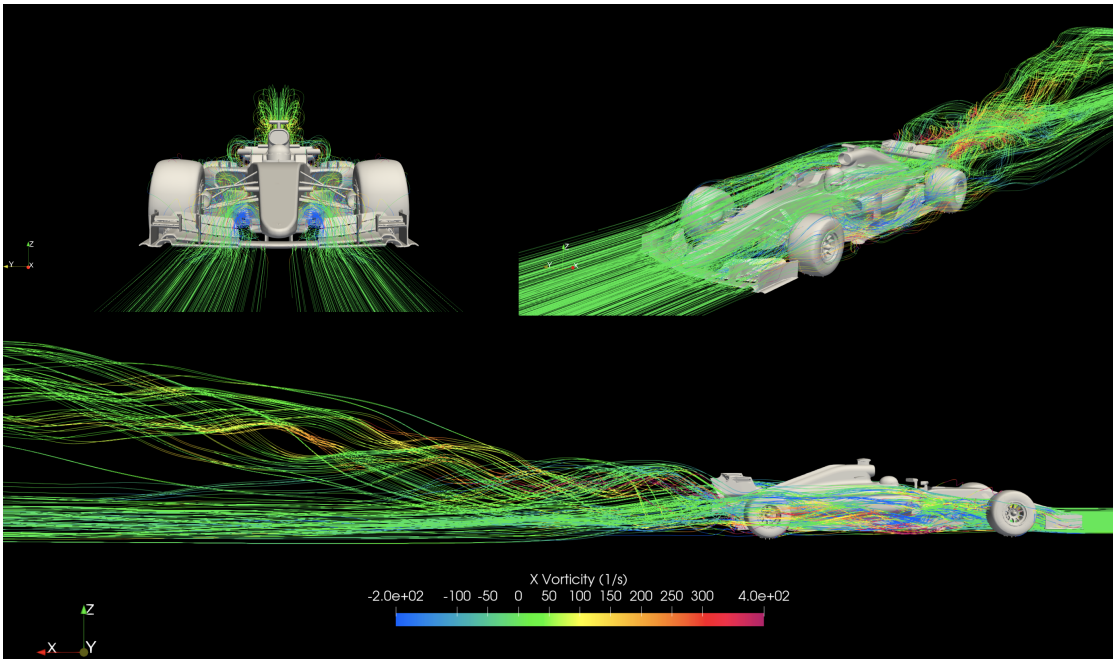

Figure 5.10: Streamlines of the axial vorticity.

Finally, the referred images (Figure 5.10) show a three dimensional representation of the **streamlines of the vorticity**. The 3 graphics differ in the origin point of feeding the streamlines, the resolution and the length of them. It is possible to see in general traits how the flow behaves around different areas of the car (Y250 vortex, tip of the wings, middle section) and how **chaotic and and turbulent** the resulting **wake** looks like.
This somehow anticipates the problematic found while driving under the wake effects of a leading car, which is deeply studied in Chapter 6.

5.6 Conclusions

By means of a CFD study, the aerodynamic performance of a F1 2017 spec. car was analysed. The main problems regarding the mesh generation were found in the **complexity of the geometry**, which required several clean-up and correction operations (5.1). After that, a brief **GCI** study was performed in order to guarantee that the results obtained were independent of the mesh size (5.3). In terms of the simulation process, the incompressible RANS equations were solved by means of the **simpleFoam** algorithm as well as the **k-ωSST** turbulence model (5.4).

The results obtained regarding the aerodynamic coefficients **encountered a close agreement** with the reference data [64]. This allowed a further study analysing the **relative contribution** of different components of the car in terms of downforce and drag generation. It was found that the most efficient way of generating downforce is by means of the **underbody**, as it is responsible for the 60% of the aerodynamic loads with a low 15% contribution to drag. Other elements, such as the **front and rear wings** proved to be as well a powerful source of downforce generation —23% and 35% respectively—. However, both **front and rear wheels** are responsible for the main source of **pressure drag**, as they generate a huge turbulent wake around them.

It has also been proved that F1 cars use very complex devices to manipulate and canalise the airflow around them. This allows the generations of different **three-dimensional vortical structures** with various purposes, but mainly to keep the flow attached and maximise the downforce generation.

Chapter 6

Under wake flows

"Once more unto the breach, dear friends, once more;"

- William Shakespeare, *Henry V Act-III, 1599.*

This chapter is oriented to evaluate the aerodynamic performance of a **F1 car under the wake effects** caused by a leading car —slipstream situation when overtaking—.

6.1 Hypothesis and starting point

Chapter 5 showed that F1 cars are well optimised for freestream flows, with low turbulence and no physical perturbations. However, race cars are constantly performing **under wake effects** due to being racing each other. At this stage, the leading car may notably affect the flow that feeds the second car, thus experiencing a **change in its aerodynamic** performance.

The new 2021 F1 regulations —currently postponed to 2022 due to the COVID-19 effects— were born with the idea in mind of simplifying the aerodynamics of the cars in order to bring back the close wheel to wheel racing of ancient times. Several wind tunnels experiments carried on by the FIA showed that the **loss of downforce levels** in 2017 spec. were **around 50 %** at a distance equal or less

than one car length [67]. For this reason, it is considered appropriate to evaluate if the wind tunnel comments from the FIA are in line with the CFD numerical data obtained in this study.

If these results match and find a coincidence verdict, it will be possible to **evidence** that the new change in the regulations **is justified** —in terms of aerodynamic purposes—.

6.2 Geometry preparation

The methodology followed is totally analogous to the one detailed in section 5.1. The only differential point resides in the **inclusion of a second car** behind the leading one at a longitude L —where L represents the length of the car—.

Different distances will be studied, representing different cases: $2L$, L, $0.5L$ and $0.25L$ to evaluate the progression of the results obtained on each case with a proportional factor of longitude L.

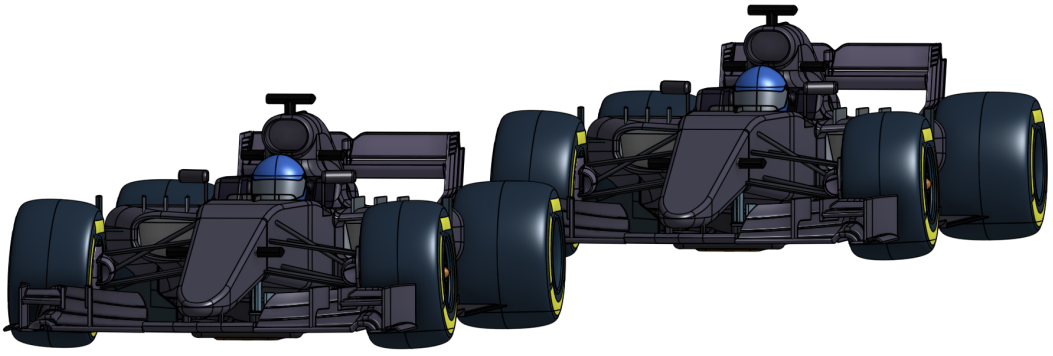

Figure 6.1: Isometric view of the 2 F1 cars.

6.3 Simulation Resources

Equally, the computational resources used are the ones presented in 5.2.

6.4 Mesh

The dimensions of the fluid domain used **remain the same** as those for the free stream simulations (See section 5.3). Previous tests on the free stream scenario —in a variety of different positions— proved that the distance between the outlet and the end of the car is **sufficiently adequate** to obtain reliable data regarding the aerodynamic coefficients.

Taking advantage of the previous work done, the meshing process followed is **analogous** to the one presented in 5.3, including the definition of boundary layers and the **GCI study** to guarantee the independence of the results. The finest mesh involved around 38M cells, which is considerably bigger than the one in the single car. Figure 6.2 reflects the mesh used in this study, special interest is placed in the **refinement enclosures as well as the wake length**. This longitude L represented is measured from the rear end of the leading car to the first contact point on the nose of the second car.

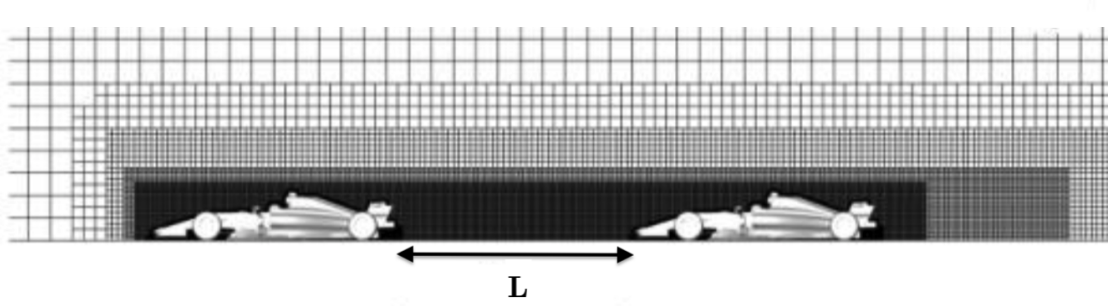

Figure 6.2: Overall mesh and refinement enclosures.

6.5 Boundary conditions and Setup

As for the boundary conditions, the **same parameters** as the ones presented in 5.4 were established. However, it was found appropiate to study here 2 different turbulent models, the **RANS** k-ωSST and the **LES** Spalart-Allmaras, to see whether any changes were appreciated in regards to the results obtained (wake development, behaviour of the second car, velocity profile, etc.)

6.6 Results

Firstly, it has to be noted that the simulation performed by means of the LES Spalart-Allmaras turbulence model resulted in a **concerning non-clear convergence** of the results; consequently, the simulation performed was considered unreliable and inaccurate. The main reason for this issue could possibly be due to the complicated geometry (ResearchGate [68]) as well as the extra amount of resources that are required (See 3.3.2).

For this reason, only the results obtained with the **k-ωSST model** are evaluated.

Aerodynamic performance

Again, the results obtained deal with the **aerodynamic coefficients**: Downforce (SC_L), Drag (SC_D), overall aerodynamic efficiency E (C_L/C_D) and Front Balance FB. Here, the latter plays an important role as its quantification enables a short study of the vehicle stability.

Tables 6.1 and 6.2 display the evaluated parameters of the second car (Follower car) as well as the percentage of change of those with respect to the first car (Leading car).

Distance	SC_L (m^2)	SC_D (m^2)	$\lvert C_L/C_D \rvert$	FB (%)
0.25L	-1.30	0.69	1.88	53
0.5L	-1.57	0.81	1.95	56
1L	-1.97	0.91	2.16	58
2L	-2.62	0.99	2.65	51

Table 6.1: Aerodynamic coefficients of the second car.

Distance	SC_L (m^2)	SC_D (m^2)	$\lvert C_L/C_D \rvert$	FB
0.25L	-62 %	-40 %	-37 %	+28.5 %
0.5L	-54.1 %	-30.7 %	-34 %	+35.8 %
1L	-42.3 %	-21 %	-27 %	+40.7 %
2L	-23.5 %	-14.2 %	-11 %	+26.1 %

Table 6.2: Percentage of change of the aerodynamic coefficients of the second car as regards the first car.

The results obtained show that the **reduction in the aerodynamic coefficients** is clearly visible from an initial distance of 2 car lengths —approximately 10.6 meters— to the closest case studied of 0.25L —less than 1.5 meters—. The reduction of **downforce** ranges from a **-23.5 %** to a very significant **-62 %** in the worst case scenario.

In a similar progression, the **drag is reduced** from a **-14.2 %** to a **-40 %** and for this reason, so does the overall efficiency of the second car.

Besides to the distinguished loss of downforce, there second car experiences a **dramatic increase of front balance** (FB) **from +26 % to 40 %**. This sudden increase on the front aerodynamic loads may presumably lead to experiencing oversteer [1] and safety issues while braking and on high-speed corners.
In general traits, it can be seen that the overall **performance** of the second car **worsens** as it approaches and gets closer to the leading one.

Figure 6.3 is aimed at showing the obtained data in a visual representation so that is possible to appreciate the rate of change in the various studied parameters.

[1] Oversteer is caused when a car steers more than intended, thus losing the rear end.

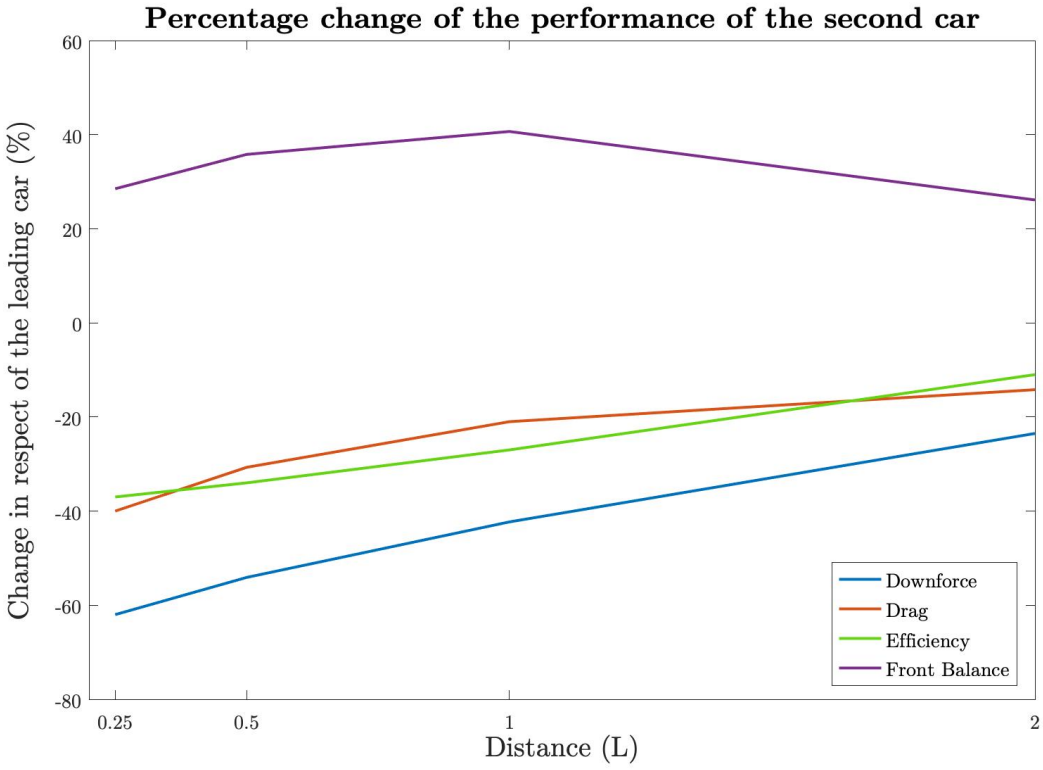

Figure 6.3: Percentage change of the performance of the second car in respect of the leading car.

As previously mentioned, the increase of the front balance levels on the second car enables a short but rather **interesting discussion**. It is known that the weight distribution of a F1 2017 specification car is around 45.5 % on the front axle [69], so the car is not supposed to exceed this 45.5 % of front balance as it may lead to stability concerns. The Center of Pressure, which by definition is such where the total sum of pressure fields act on, **should always remain behind the Center of Gravity**. This can be explained as the yawing moment of the aerodynamic forces counterbalances the steering of the driver and therefore **stabilises** the car. On the other hand, if the Center of Pressure is ahead of the Center of Gravity, the yawing moment increases the sidesplip angle and produces **instability**. Figure 6.4 shows that dynamic behaviour.

As the results obtained show, the front balance of the second car adopts always values that are greater than 45.5 % (See Table 6.1). This implies not only a **reduction of the stability and the performance** of the car —slower laptimes

and more degradation of the front tires— but also a more **challenging approach** when driving the car; major ease of spinning and safety issues.

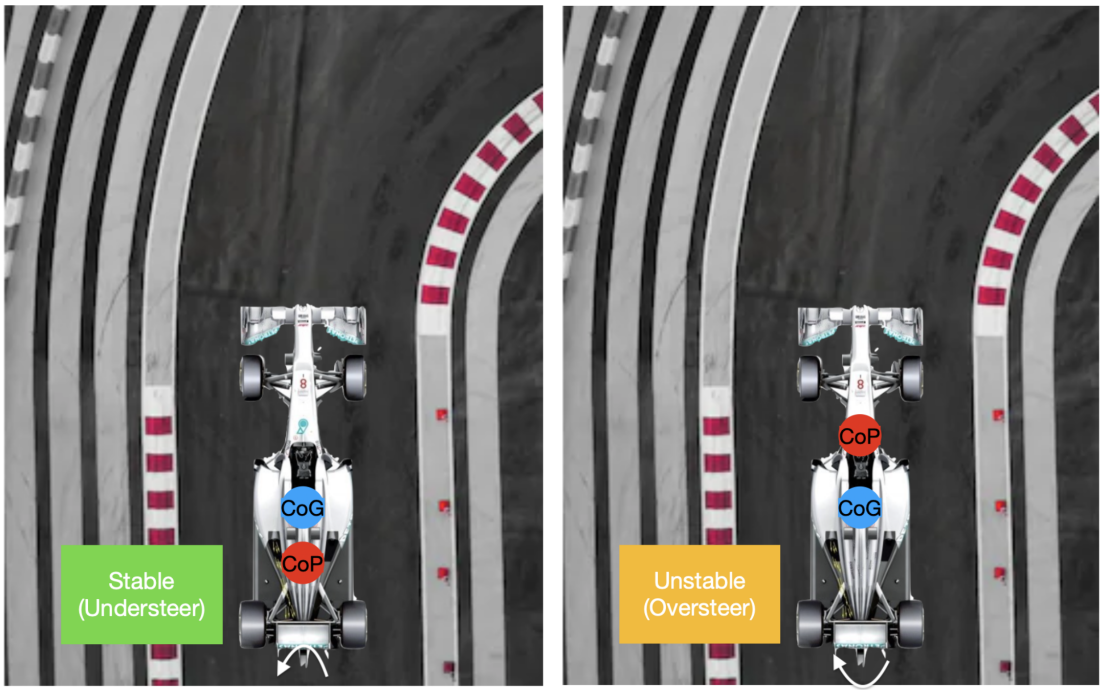

Figure 6.4: Stable and Unstable scenarios dictated by the relative position of the Center of Pressure.

Moreover, the study analyses the **performance of the most relevant aerodynamic devices** on the follower car: Front wing, rear wing and diffuser. Tables 6.3, 6.4, 6.5 and Figure 6.5 show the mathematical results obtained.

Distance Front Wing	SC_L (m^2)	SC_D (m^2)
0.25L	-38 %	-36.1 %
0.5L	-29 %	-19.3 %
1L	-10.7 %	-1.1 %
2L	-3.6 %	+3 %

Table 6.3: Percentage of change of the aerodynamic coefficients in the front wing of the second car as regards the first car.

Distance Rear Wing	SC_L (m^2)	SC_D (m^2)
0.25L	-57.9 %	-53.3 %
0.5L	-54.8 %	-50.6 %
1L	-52 %	-48 %
2L	-40.3 %	-36.2 %

Table 6.4: Percentage of change of the aerodynamic coefficients in the rear wing of the second car as regards the first car.

Distance Diffuser	SC_L (m^2)	SC_D (m^2)
0.25L	-70.2 %	-57.2 %
0.5L	-62.8 %	-48.7 %
1L	-46.1 %	-29 %
2L	-25.3 %	-16.9 %

Table 6.5: Percentage of change of the aerodynamic coefficients in the diffuser of the second car as regards the first car.

Table 6.3 reflects that the loss of downforce of the front wing starts to **appear severely at a distance of 1L** up until a **very critical -38 %** when it reaches 0.25L.

On the other hand, drag levels are found to be grater than the leading car at a distance of 2 car lengths, but a similar behaviour to the downforce is found as long as the distance is decreased. This could be explained due to the **turbulent conditions** that are found far away from the leading car. Moreover, as the second car approaches the leading one, it enters into a **very strong wake region** that hits initially the front wing and eventually influences all the behaviour of the car.

As shown in Table 6.4, the behaviour of the rear wing is notably different: the **loss of downforce is very notable** since the very first distance of $2L$ and keeps increasing as the slipstream distance gets closer. Similarly, the drag levels are also reduced strongly from the beginning and matching a comparable ratio that keeps the **efficiency almost constant**.

It can be stated then, that the **rear wing is more affected** under the wake

effects than the front wing, as the latter seems to suffer less and only under close proximity. This somehow explains the **increase of front balance** —and forward change of the center of pressure— and its posterior decrease as sketched in 6.3.

Finally, Table 6.5 reports that the **diffuser** is the device that **suffers the most under the wake conditions**, as the downforce loss in close proximitiy is around **70 %** and the drag is found the be reduced around **57 %** at the same distance. However, the interesting conclusion is that the reduction of downforce starts from the very first beginning and keeps increasing as the distance is reduced. This evidences that overtaking maneuvers are **heavily influenced** since the start —as it is important not to forget that the diffuser is the greatest source of downforce generation as seen in Section 5.5—.
This generates an interesting and deep discussion, as it is encountered that the greatest way of generating aerodynamic loads under a free stream flow, is at the same time the **worst one** under wake flows. The whole conception and functioning of the underbody is found to be absolutely **pointless**; therefore other aerodynamic paths and solutions should be evaluated if these losses are wished to be recovered.

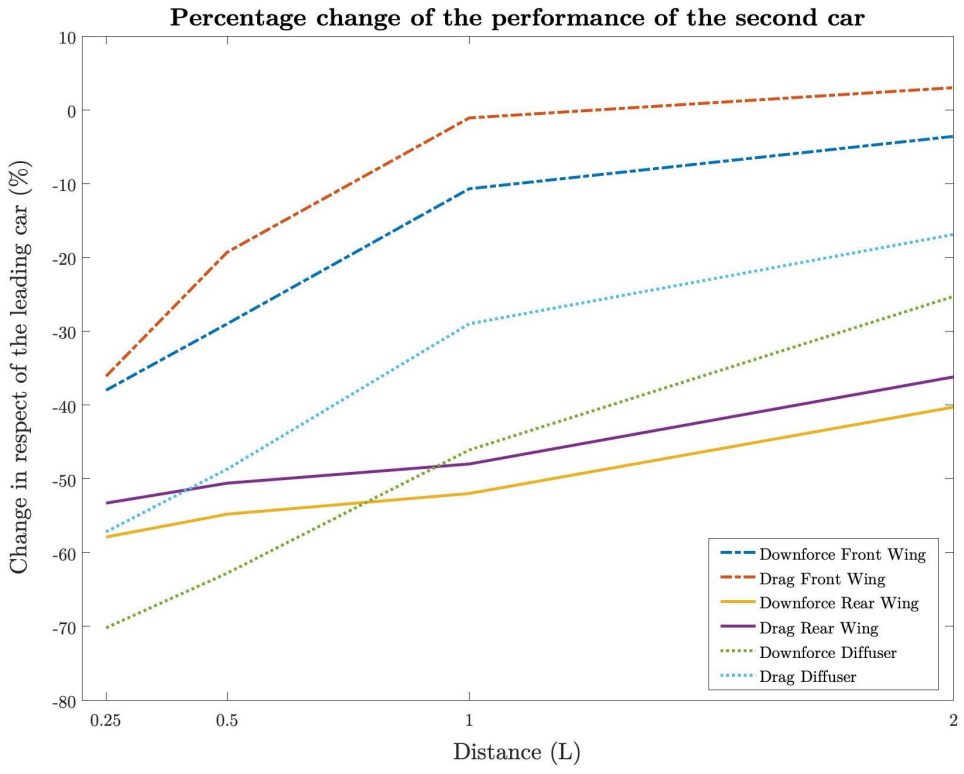

Figure 6.5: Percentage change of the performance on the aerodynamic devices of the second car in respect of the leading car.

Pressure distribution

The present section deals with several **pressure coefficient** (Cp) plots that help understand the overall performance of the different parts of the car. All these plots are referred to and **portray the second car** under the wake conditions.

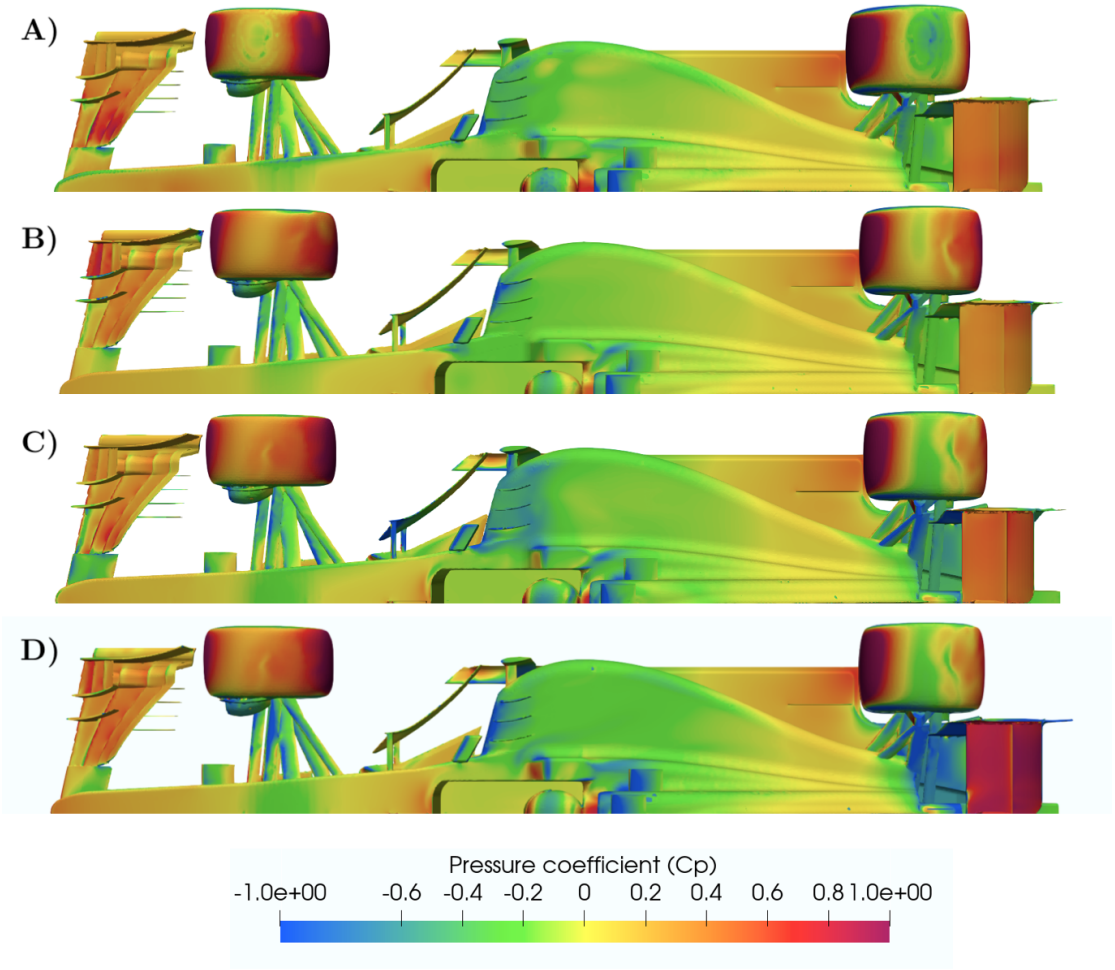

Figure 6.6: Pressure coefficient distribution related to the second car at a distance of A) 0.25L, B) 0.5L, C) 1L and D) 2L.

Figure 6.6 sketches how the aforementioned comments made earlier in Section 6.6 are here present in terms of pressure distribution. From an early stage, the **pressure loss** in the **rear wing** is severely and gradually **appreciated**. The approach to the leading car **damages distinctly** the functioning of both its stabilising and suction purposes.

Furthermore, it is possible to note that bargeboards and vortex generators located on the top of the sidepods **diminish its efficiency** since the pressure distribution around the bodywork reflects greater gradients as the second car approaches the leading one.

On the other hand, it is found appropriate to include as well the pressure distribution of the front wing and diffuser of the second car. Figure 6.7 shows precisely the behaviour commented earlier as the low pressure zones of the **front wing suffer an abrupt change** and loss as the car enters into the closer wake region (cases B and A). These changes are noticeably **far less progressive** than the rear wing's, which evidences as well the premature **front balance shift**, but allow a more robust behaviour at greater distances.

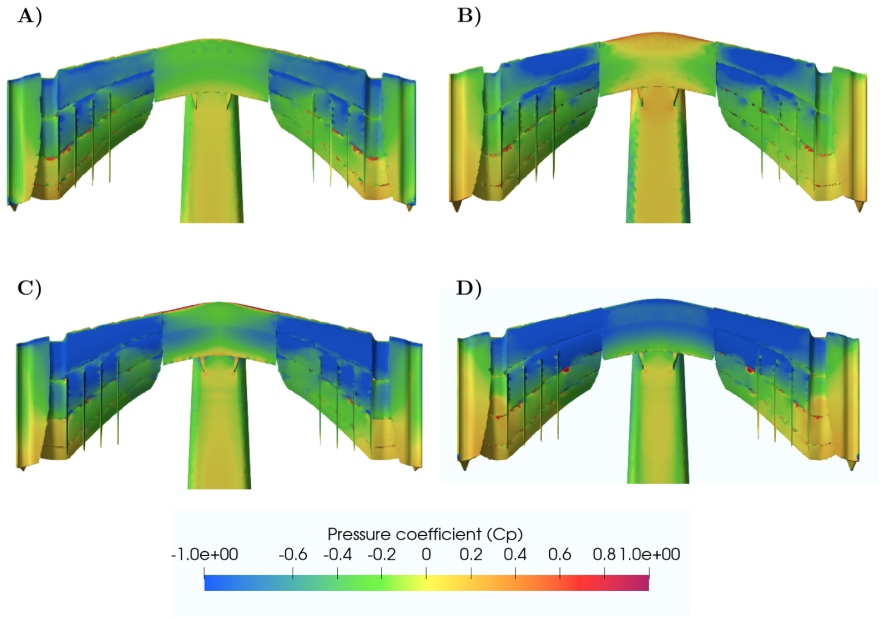

Figure 6.7: Pressure coefficient distribution on the front wing of the second car at a distance of A) 0.25L, B) 0.5L, C) 1L and D) 2L.

On the diffuser side, the results again show that the whole low pressure zone is affected since the very first beginning, with **moderate areas** near the diffuser strakes with higher pressure values.
However, the **degradation** of the performance is perfectly noticeable and proves again that the diffuser **suffers excessively** under wake flows until its contribution becomes almost negligible.

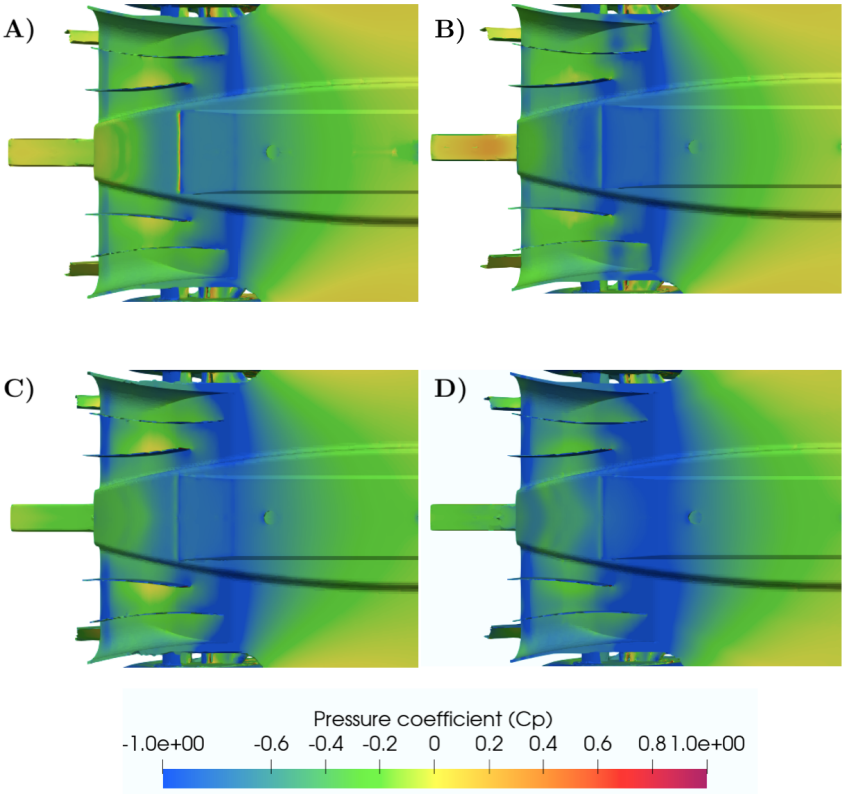

Figure 6.8: Pressure coefficient distribution on the diffuser of the second car at a distance of A) 0.25L, B) 0.5L, C) 1L and D) 2L.

Wake and velocity contours

Figure 6.9 portrays a lateral view of the velocity contours created under the wake flow. All 4 scenarios studied are represented so that the reader may appreciate the differences among them.

It is possible to see that the second car is affected by a flow which is **lower in terms of kinetic energy**, as the wake generated by the leading car is released far away disturbing its follower. It is clear as well, that as the second car gets closer, it inherently enters into a unique wake structure characterised by very low speed flow —that ranges from 0 to 10m/s—, therefore, resulting **severely affected**.

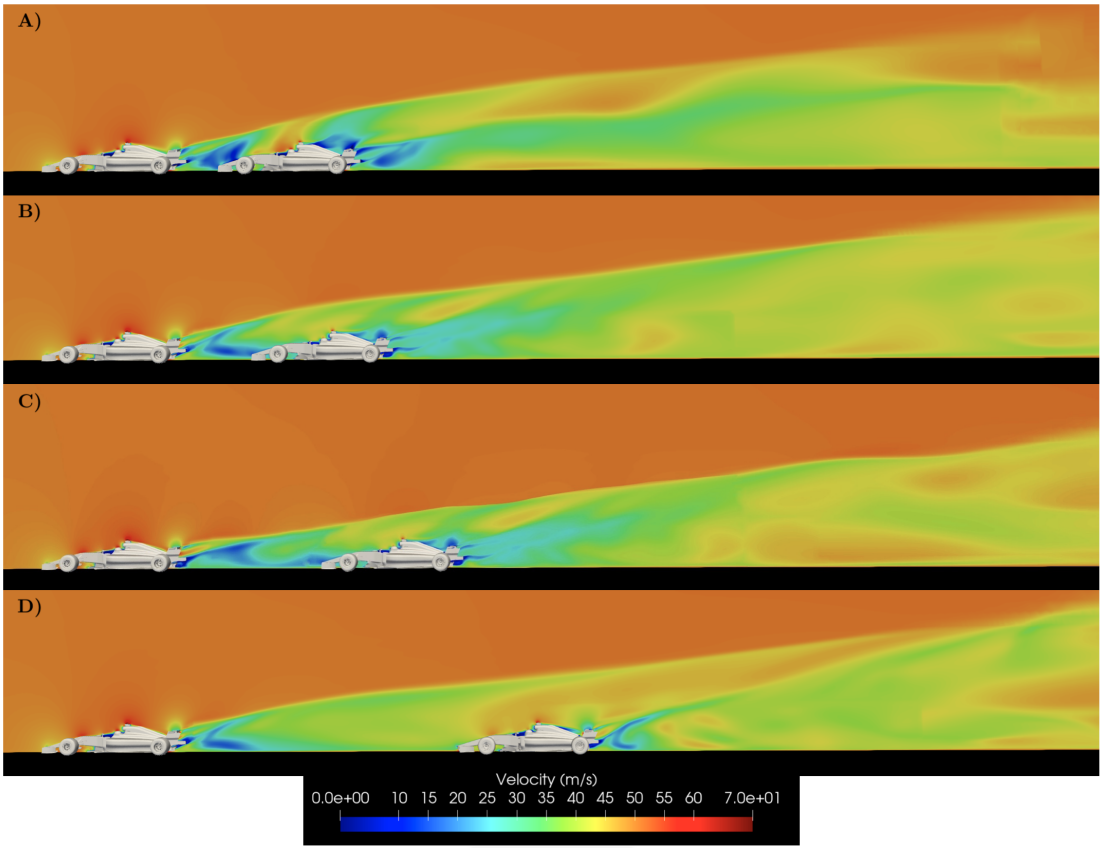

Figure 6.9: Velocity contours on the symmetry plane at a distance of A) 0.25L, B) 0.5L, C) 1L and D) 2L.

On the other hand, Figure 6.10 displays a top view of the same 4 scenarios that intercept the flow feeding the front wing and exiting the diffuser. It is seen that as the second car reduces the distance, its wake originates a separation region that enlarges and becomes evident as the distance is closed. At a large distance (2L), the second car's wake adopts a **needle shape**, which somehow imitates the free stream natural wake, but this shape **soon disappears** at closer distances.

As for the leading car, it can be noted that its wake is not notably modified —in terms of shape and contours— by the presence of the follower car. The aerodynamic coefficients evaluated on the leading car only experience a **low variation** —less than 3%—, when the distance between the two cars is set at 0.25L.

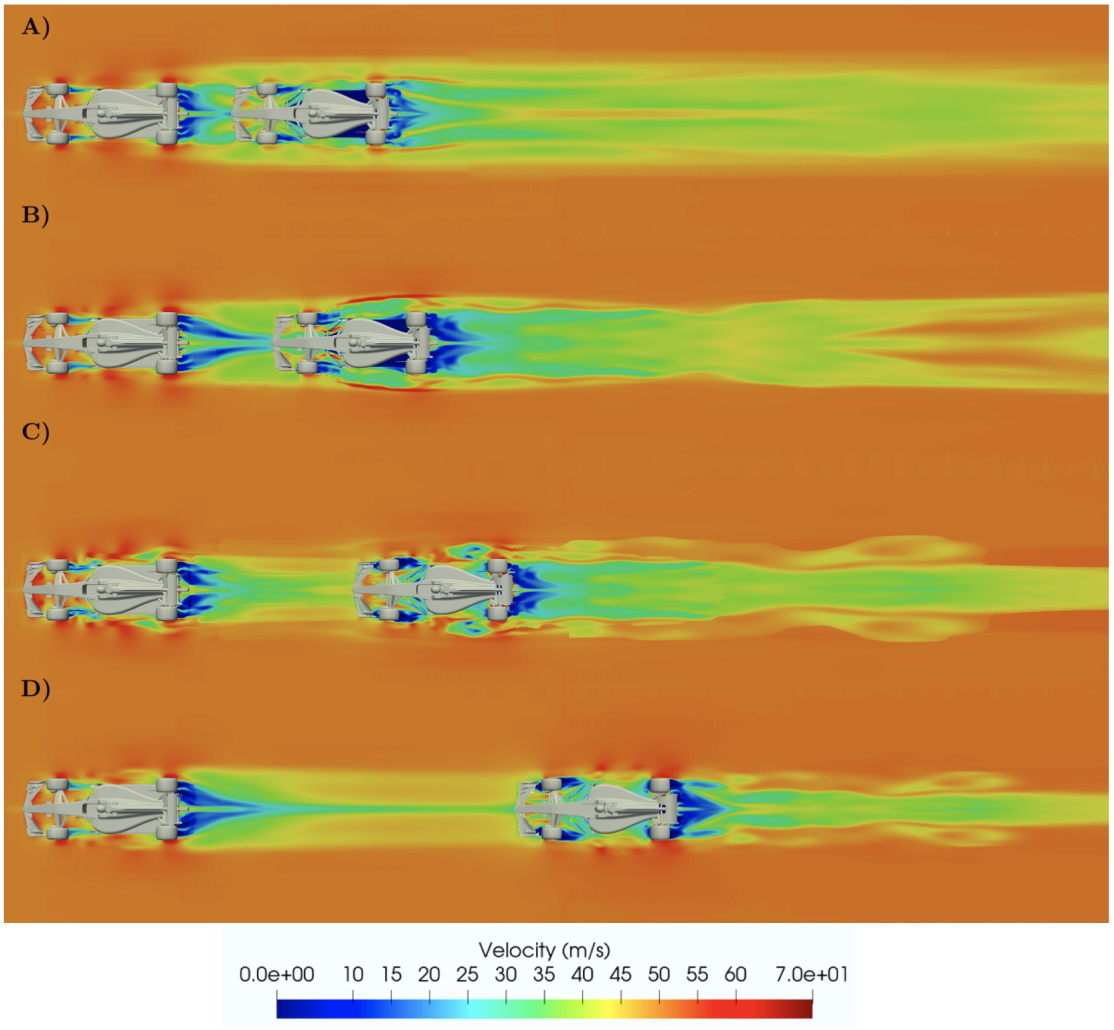

Figure 6.10: Velocity contours on a top plane at a distance of A) 0.25L, B) 0.5L, C) 1L and D) 2L.

Shifting now to the streamlines of the velocity, Figure 6.11 displays 2 different planes for each scenario. The first thing one may notice is how the **airflow is perfectly attached** to the first car; from the front wing, going through the sidepods and bodywork and finally exiting the rear wing.

However, it is possible to see as well, that the exiting airflow on the rear-end of the leading car is somehow **divided into two** characteristic flows: the first one, located on the superior area, which adopts high-speed values due to being **accelerated** around the bodywork (low pressure zone and smooth behaviour) and the second one, which exits the diffuser upwards and is mainly a **turbulent flow** continuously undergoing changes in both magnitude and direction.

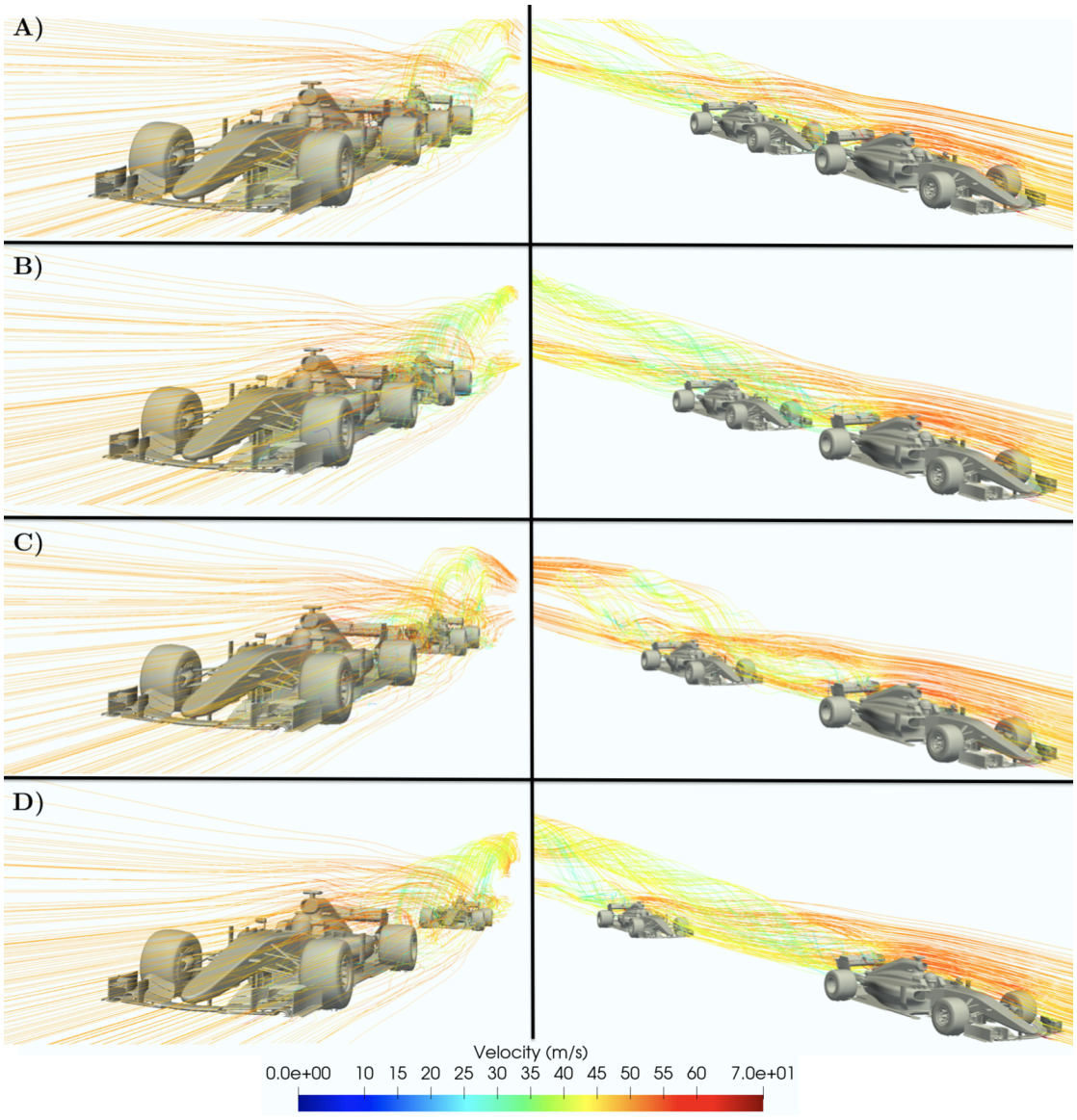

Figure 6.11: Streamlines of the velocity at a distance of A) 0.25L, B) 0.5L, C) 1L and D) 2L.

The mixture of the previously mentioned flows is what originates such a chaotic wake region, as it is formed by the combination of **multiple flows** with various natures and velocities [70].

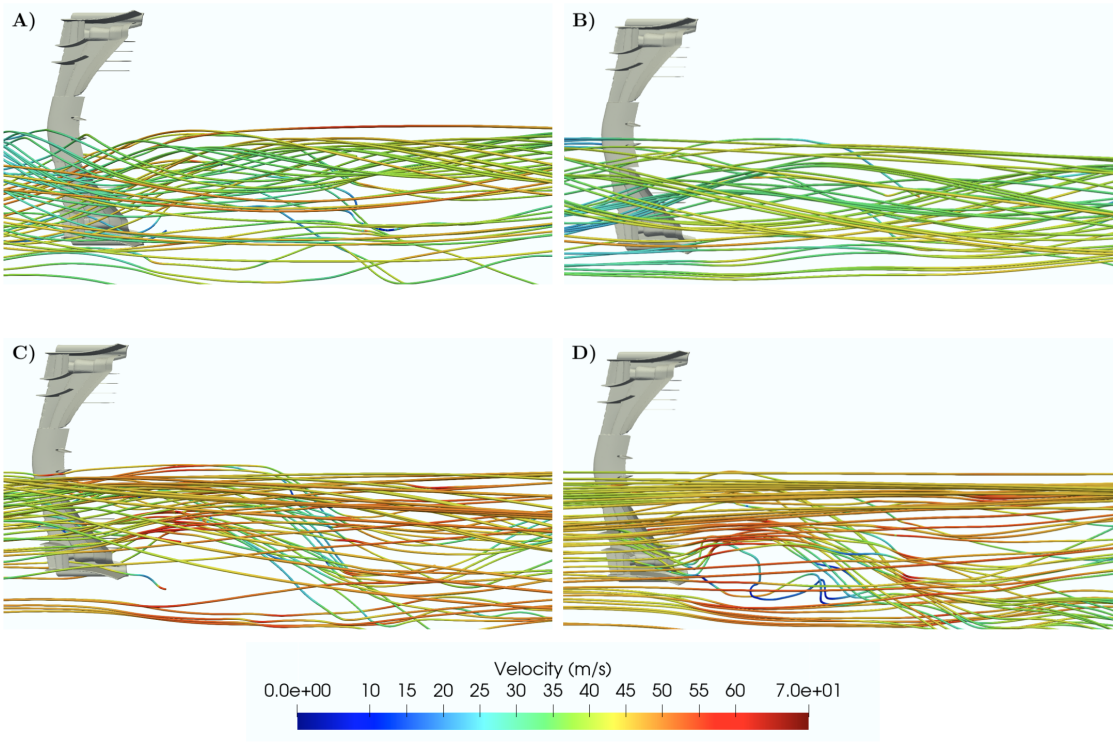

Figure 6.12: Streamlines of the velocity. Front wing of the second car at a distance of A) 0.25L, B) 0.5L, C) 1L and D) 2L.

Figure 6.12 presents the streamlines of the velocity feeding the front wing of the follower car at different distances so as to appreciate the main differences among them.

Scenario 6.12 D) shows that the magnitude of the **velocity is somehow similar** to the one of the free stream flow —although it presents low velocity areas on the central part of the wing—. However, endplates and wing tip elements are still useful to redirect the flow towards the rear. As the distance is halved, the velocity of the flow is **reduced** and the front wing **loses its capacities** to govern the airflow, but it is not until cases A) and B), that the front wing is fed by really low kinetic energy flow that leaves it **notably inoperative**. The effectiveness of the generation of vortices and the redirection of the flow is insignificant, just as predicted in Table 6.3 due to the strong wake region.

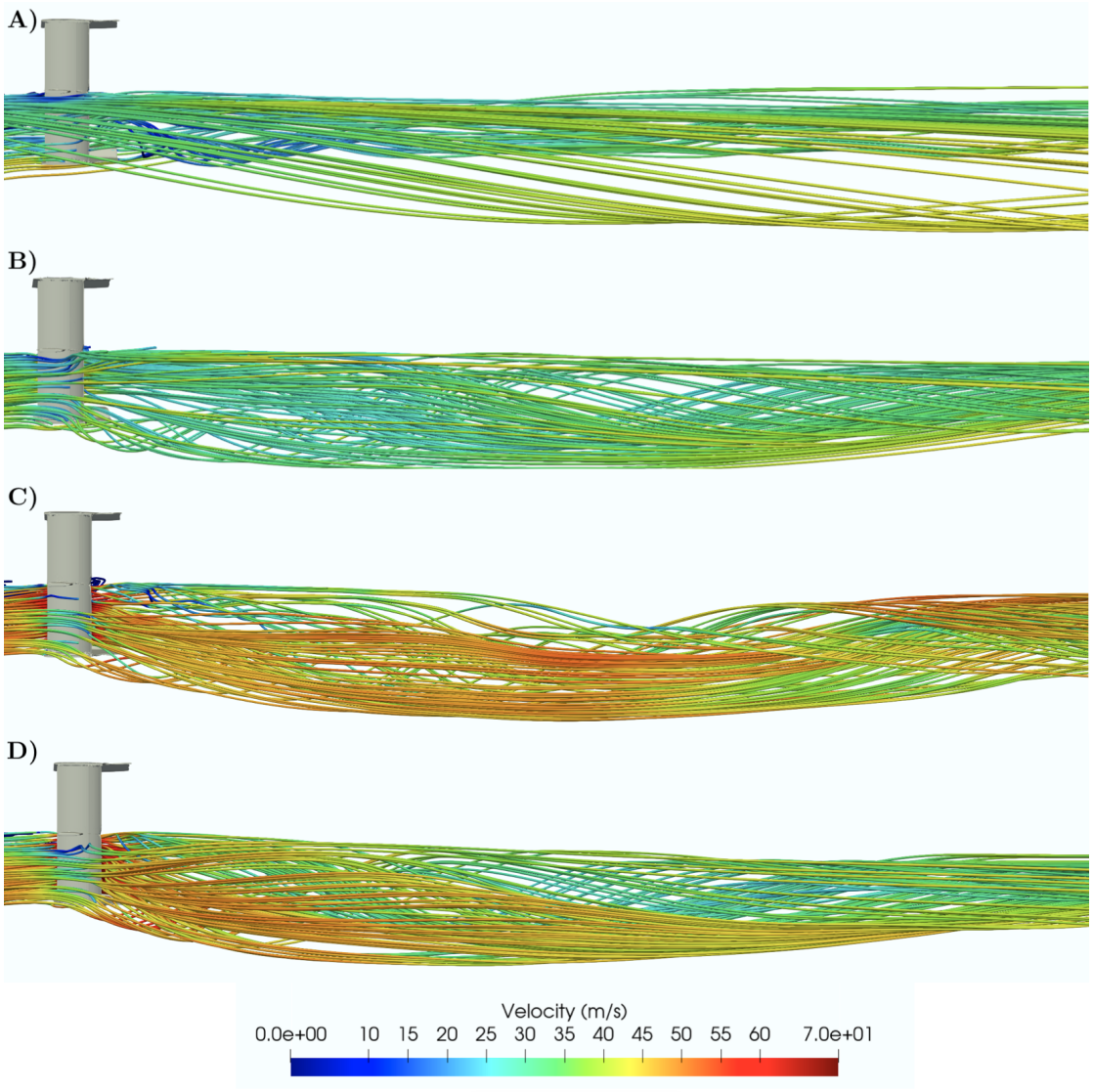

Figure 6.13: Streamlines of the velocity. Rear wing of the second car at a distance of A) 0.25L, B) 0.5L, C) 1L and D) 2L.

Moving into the rear wing, the same comparison is conducted and shown in Figure 6.13.

Under a normal regime, the rear wing works perfectly with aligned flow redirected by other aerodynamic devices, but it is possible to see that as the distance is reduced, the **streamlines tend to deflect slightly inboard**. The clear jump in terms of velocity magnitude is produced from case C) to B), where the flow experiences a moderate **deceleration** as it enters into the strongest wake region. It could be speculated that the rear wing is more sensitive to the direction of the

flow than the front wing due to its low aspect ratio, the pronounced curvature and the massive endplates at both sides. Scenario 6.13 A) shows a mixture of velocity flows with very low speed that **unexpectedly create an inwash phenomena** at the rear end of the wing. This evidences that the whole aerodynamic package of the follower car is prominently disrupted under the wake conditions.

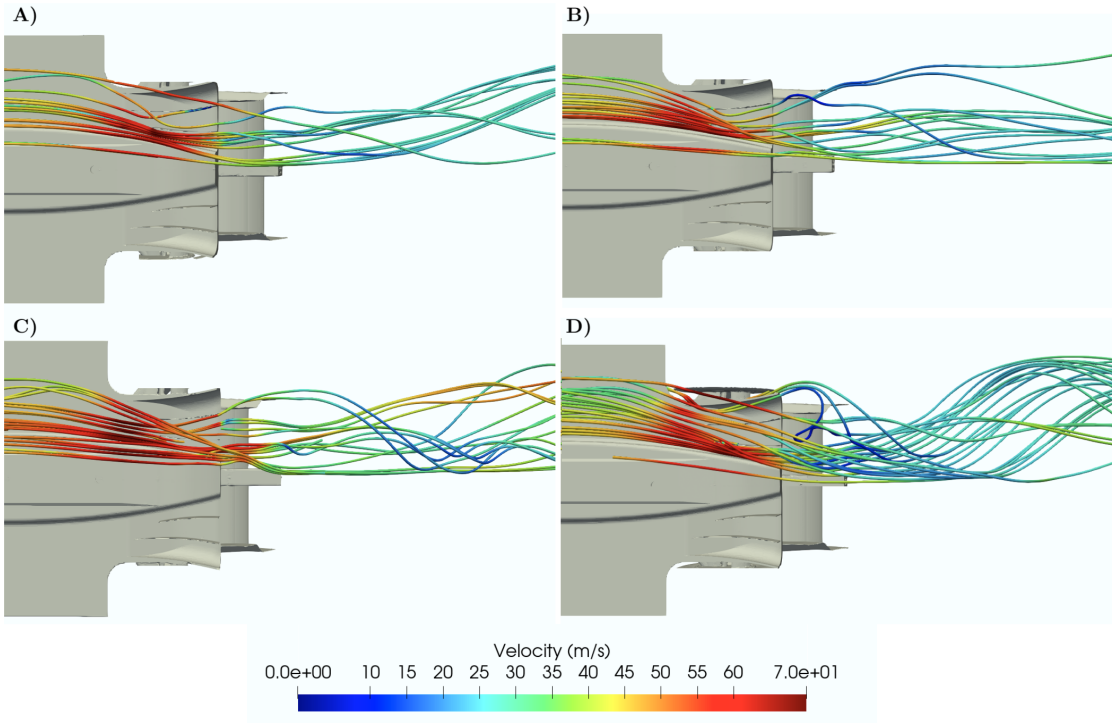

Figure 6.14: Streamlines of the velocity. Diffuser of the second car at a distance of A) 0.25L, B) 0.5L, C) 1L and D) 2L.

Finally, Figure 6.14 describes how the underbody, and particularly the diffuser is affected by the wake flow. In free stream conditions, the diffuser is fed by a **high energised** flow redirected by the front wing and guided around the flat floor. Nonetheless, the streamlines of the flow are not completely straight as the vortices management allow the control of the airflow around the underbody. Scenario 6.14 D) displays a quite non-disturbed behaviour of the airflow as the **management** of it **is still acceptable**. When the distance is reduced, the performance of the underbody **starts worsening** due to the flow arriving more disturbed into the diffuser hence, not being able to operate properly. Smaller distances such as cases B) and A) reflect an underbody region fed by a **very low kinetic and**

rotational flow. The main reason for the massive downforce losses reported in Table 6.5 is that the underfloor is notably sensitive under wake flows, as it **works closer to the ground** than the front wing. This means that the low energy —and highly-rotational— airflow may not be compressed around this small area, therefore experiencing a **massive performance loss**.

6.7 Conclusions

The goal of this chapter was to evaluate whether the current F1 cars would necessarily require an aerodynamic update due to its difficulty to perform under wake flows. Having accomplished the simulation and evaluation of second study, it can be stated that **F1 cars are well optimised** for free stream conditions, but **suffer huge aerodynamic losses** when running under **wake flows**.

As reported, the **loss of downforce** noted ranges from 23 % —when running at a distance of 2 car lengths—, to a very significant 62 % —at a distance of a quarter car length—. This implies that the follower car encounters a quite **harsh difficulty** when trying to perform an overtake, as the aforementioned loss of aerodynamic loads prevents it from running closer to its predecessor.

Furthermore, it has been proved that the **Center of Pressure** (CoP) experiences a **shift forwards** as the second car approaches the leading one, which not only implies a reduction of the stability and performance, but also a more dangerous behaviour and safety issues.

In regards to the individual focus placed on the different aerodynamic devices, it has been found that the **front wing** experiences a **sudden jump** on downforce losses only when it enters into the closer wake region. On the other hand, the **rear wing** suffers massively from long distances, but its **losses are way more linear** and moderate. As for the **diffuser**, it is found that it represents the **most affected** aerodynamic device, as its performance is reduced from a considerable 25 % to a huge 70 %. This evidences that the conception of the diffuser and vortex management under the floor becomes critically compromised under wake flow conditions.

Finally, more evidence in form of plots, graphics and images has been provided to evaluate and conclude that the study performed **encounters a good agreement** with the FIA comments [71]. For this reason, it can be stated that the change in the current regulations is considered to be **adequate**, **necessary** and **justified** in terms of aerodynamic performance.

Part IV

Evaluation

Chapter 7

Economic summary

The full economic summary of this study is attached in the **Budget document**. There, the total cost and its distribution is detailed and fragmented for a better understanding and comprehension.

The sum of all the economic categories adds a total cost of **fifteen thousand five hundred and ninety euros** (15590 €).

Chapter 8

Environmental impact

The environmental impact of this study is clearly **minimum** as all the actions performed do not undertake prototyping tests nor experiments out of the simulation environment by means of a personal laptop.
This is so, as the study is done with the object to be the prior step to a valid approximation of a complex and real issue. Therefore, **no environmental damage** is caused within its execution.

Chapter 9

Planning and scheduling

Planning and scheduling are **two essential stages** to consider when carrying out a project or study of a certain magnitude. The present study was planned and scheduled bearing in mind that it should take **600 hours** to be completed. For this reason, it was believed that a weekly distribution would potentially adapt better to such a scheme, organising the aforementioned 600 hours within 20 working weeks. Figures 9.1 and 9.2 display the Gannt diagram that was initially planned.

It is important to note that although the majority of the tasks and the overall planning **was followed adequately**, several tasks involved a **major dedication** in terms of time and resources. These tasks; such as the meshing procedures and the simulation times adopted a volatile behaviour as they were hard to predict, quantify and schedule. The need for further refinements, divergence issues or even exceeding the limited core-hours resulted in a slight modification of the pace and timing of the project, but always **within the limits** of the predicted estimations.

Finally, it can be stated that all goals and targets planned initially **were accomplished** successfully due to the adequate scheduling and parallel tasking.

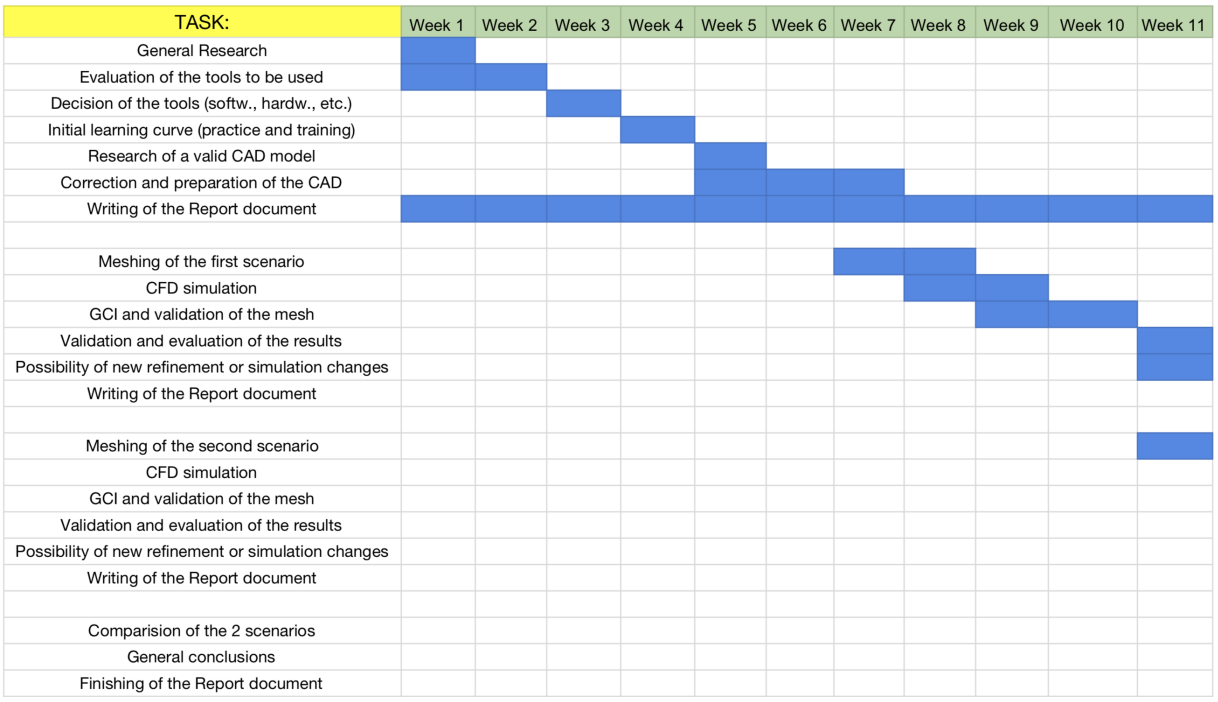

Figure 9.1: Gannt diagram from Week 1 to Week 11.

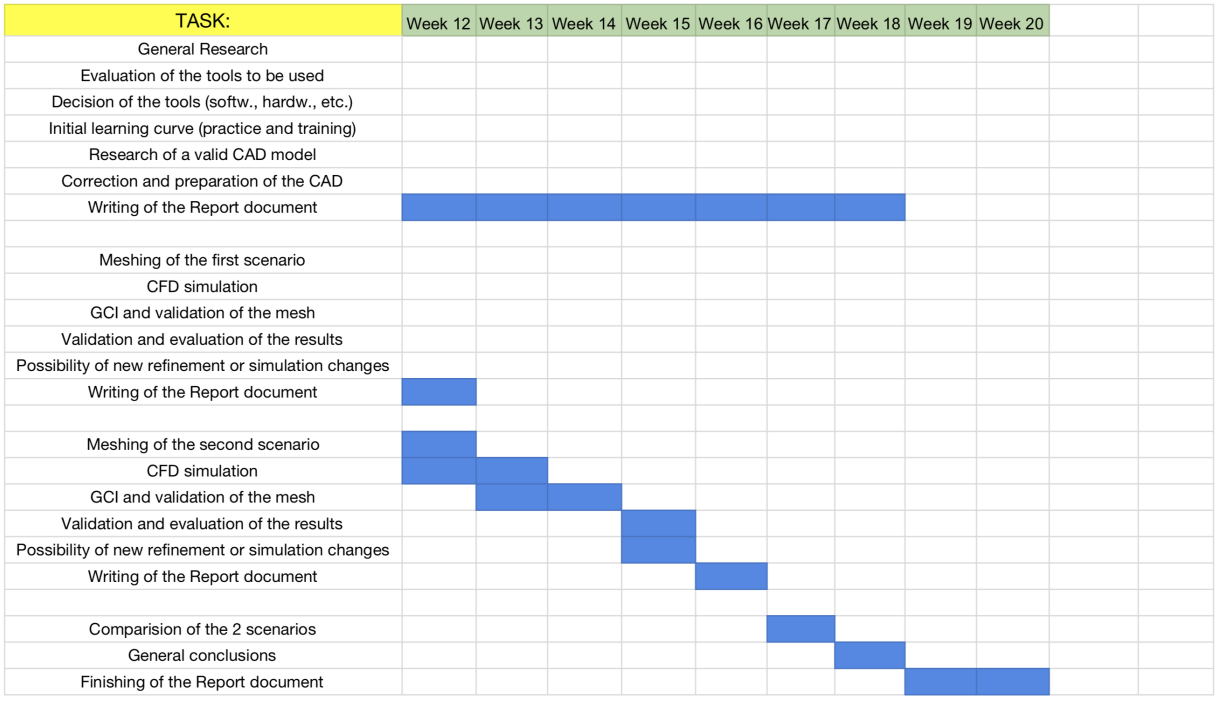

Figure 9.2: Gannt diagram from Week 12 to Week 20.

Chapter 10

Final conclusions

Formula One is with no hesitation the most challenging motorsport category in the world. Millions of Euros are spent every year within the budget of Formula One teams, specially in the aerodynamic development.

The initial point of the present study was to establish whether the current F1 regulations required an **urgent change** in order to objectively improve the category. In other words, to test and validate that the upcoming regulation changes are justified aerodynamically. The pretext was clear, direct and concise.

Two major scenarios, —or flow conditions— were studied; the first one involved the evaluation of a 2017 F1 spec. car under a **free stream flow**. The simulation offered several interesting results: the aerodynamic performance of the car **encountered a good agreement** with the reference data, which validated the study and gave rise to a further discussion. It was found that the underbody of the car, —composed by a flat floor, the planck and the diffuser— was able to provide around the 60 % of the downforce of the overall car. Other elements, such as the front wing and the rear wing reported a downforce contribution of around 23 % and 35 % respectively. Besides, the visualisation of three-dimensional vortical structures allowed to understand the behaviour of modern F1 cars, being the vortices management one of the most important areas on the aerodynamic development.

However, the second scenario was based on a more compromised but very usual situation: **running under wake flows**. Four different cases were evaluated,

where the distance between the leading and the follower car was reduced from 2 car lengths —which symbolised the start of an overtake— to 0.25 car lengths —which was considered the closest condition before crashing—. The results of the simulations performed were indeed rather clear, as they reported that the **loss of downforce** experienced by the second car ranged from 23 % to a very significant 62 % in the closest case. This means that there is clearly an **important issue** when overtaking as the loss of downforce in the corners prevents a proper racing. It was also studied a usually unnoticed phenomena regarding the movement of the Center of Pressure ahead of the Center of Gravity, which involved a more **unstable behaviour** and an unpredictable and dangerous performance. As for the individual components, it was seen that elements such as the **front wing** suffer excessively under the closer wake region, as opposed to the **rear wing**, which starts loosing attributes since the very first beginning. The **diffuser** however, represents the **most affected** device as its performance is diminished to such an extent, that its benefits become insignificant.

Finally to sum up, it may be stated that modern F1 cars are designed and **well optimised to run under free stream flows**, but suffer excessively when running under wake flows. The modern performance of Ground Effect by means of vortices management represent a very unique and complex way of modelling modern aerodynamics, but at the same time compromise notably the performance of the cars when an overtaking maneuver is intended. For this reason, it is possible to guarantee that the FIA change in the current regulations is considered to be **adequate**, **necessary** and **justified** in terms of aerodynamic performance.

Future Works

Regarding the future actions, **several modifications** to the existent geometry can be made; such as the merging of the surfaces into simpler groups or the **addition** of several aerodynamic devices like a T-wing, a Shark Fin or structural add-ons such as a Halo or an Aeroscreen to give the car a more updated and complex appearance. Some of these modifications have already been performed personally and will be compared to this study to evaluate the overall performance of the cars. Appendix B shows some of these future modifications and additions.

On the other hand, a quite interesting approach could be based on the **modification of the existent** aerodynamic devices in order to evaluate how its modifications affect their performance. For example, evaluate the loss of downforce under wake flows if the rake angle of the leading car is modified, or if the diffuser dimensions are enlarged. Besides, other conceptions such as **parametric design** could be implemented, which would definitely allow for a more complex studies of the quantification on the gains or losses due to changes.

Finally, a fair comparison, both in free stream and under wake flows with a **2022 F1 configuration** would be quite interesting as it would show whether the changes in the regulations have led to an improvement or not.

Appendix A

Meshes

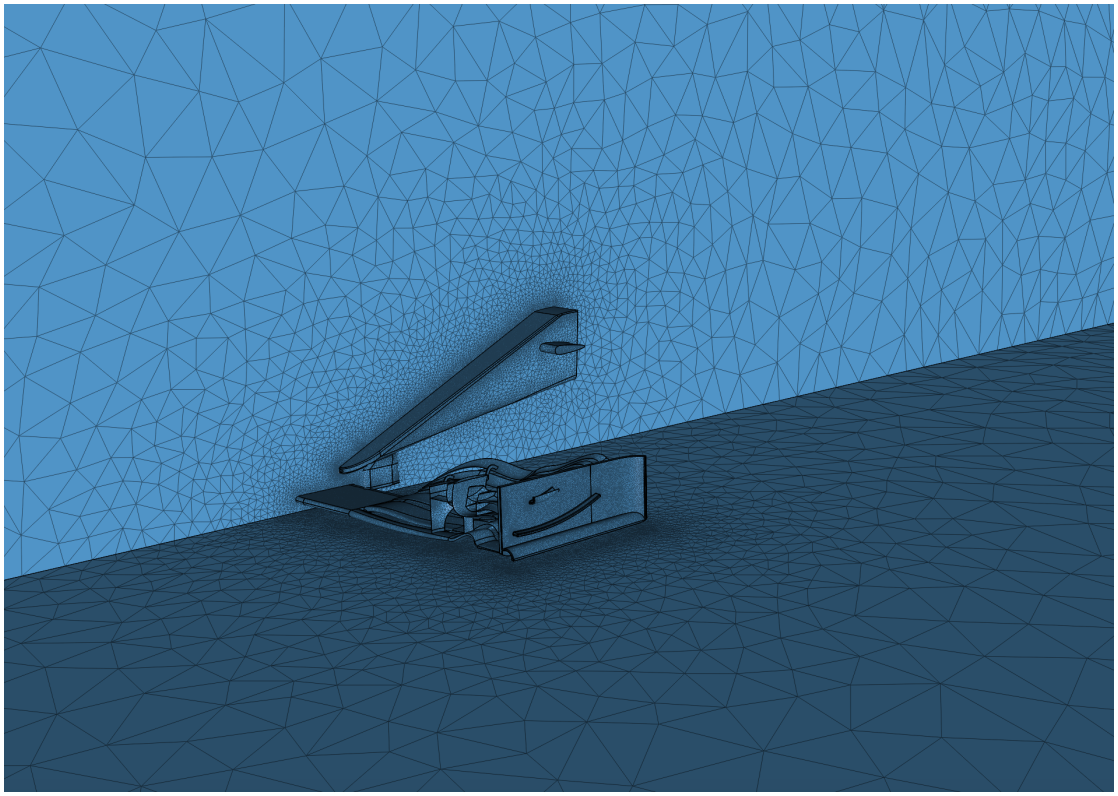

Figure A.1: Preliminary test. Tetrahedral mesh of the front wing.

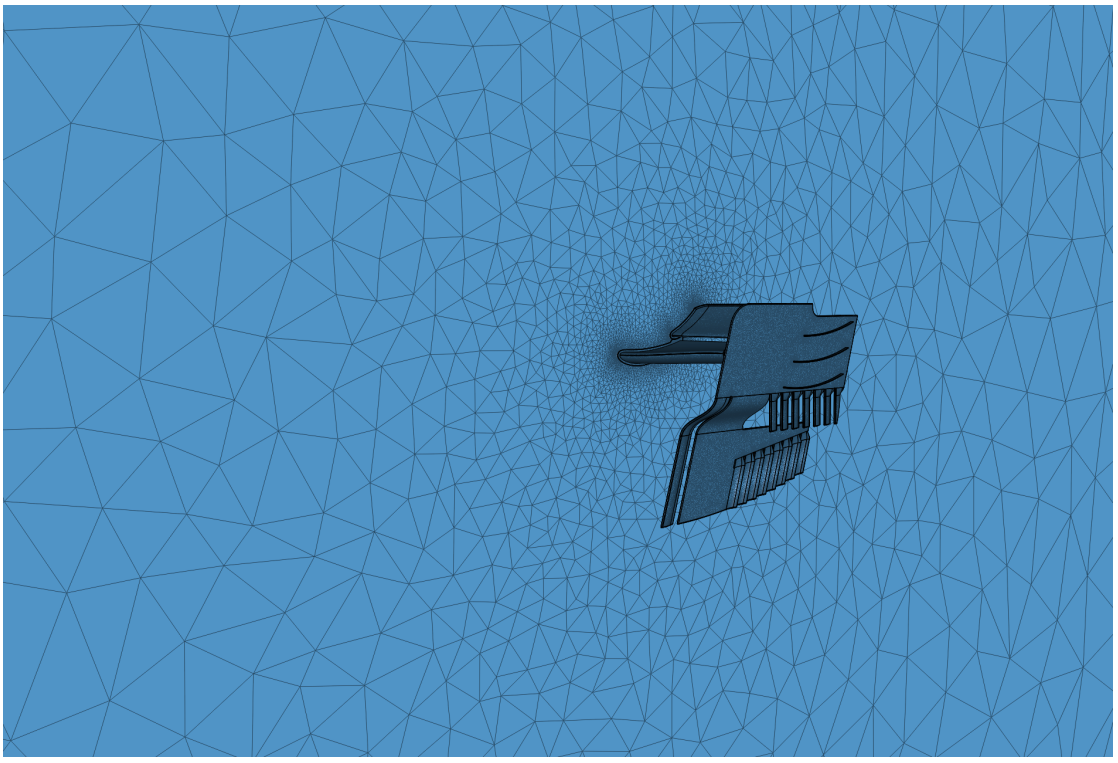

Figure A.2: Preliminary test. Tetrahedral mesh of the rear wing.

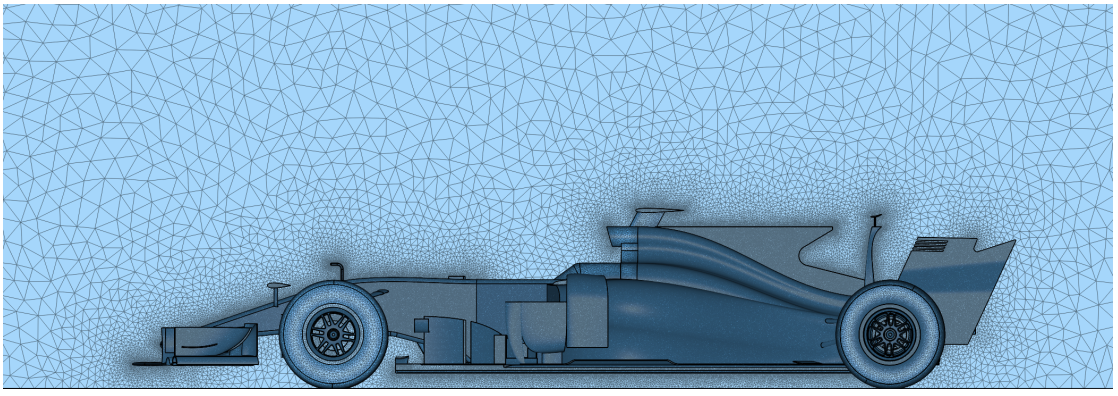

Figure A.3: Preliminary test. Tetrahedral mesh of the whole car (modified).

Figures A.1, A.2 and A.3 show the preliminary tests carried out with different aerodynamic parts by means of tetrahedral meshes. These structures were generated faster than the hexahedral ones —in terms of the meshing process— but eventually experienced more convergence problems. Besides, once the convergence issues were solved, the results obtained were slightly less accurate than ones found with tetrahedral meshes.

For this reason, some more computational cost and time was sacrificed as an exchange for a more precise and accurate solution, which led to the usage of hexahedral meshes.

Appendix B

Modifications for future works

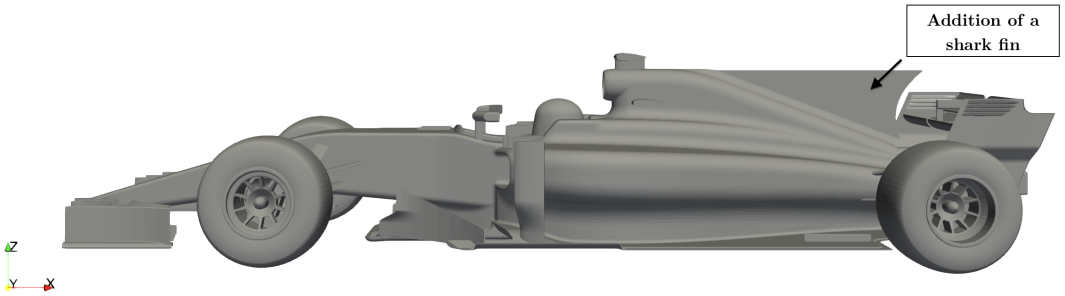

Figure B.1: Shark Fin addition for a future simulation.

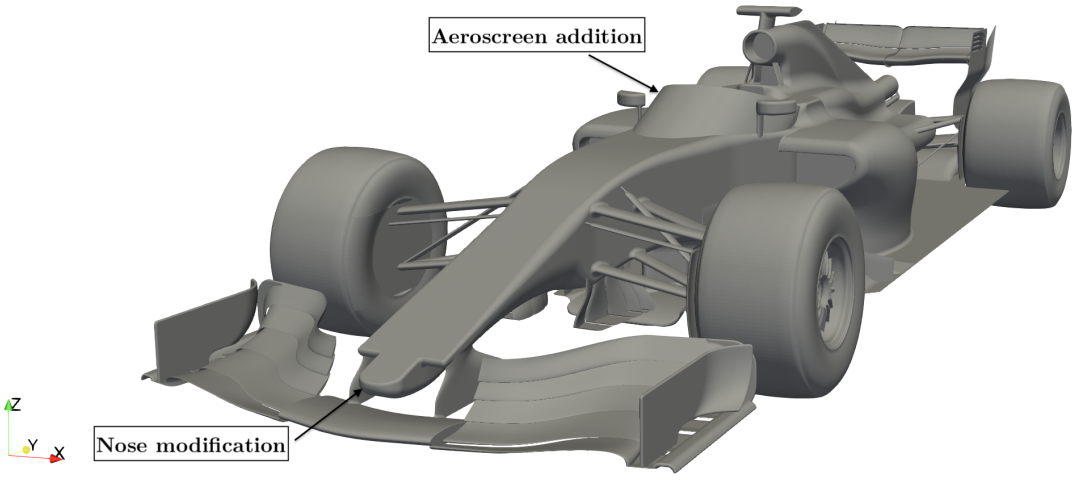

Figure B.2: Nose modification and Aeroscreen addition for a future simulation.

Appendix C

Scripts

C.1 Control Dict

```
/*---------------------------------*- C++ -*----------------------------------*\
=========                 |
\\      /  F ield         | OpenFOAM: Open Source CFD Toolbox
 \\    /   O peration     | Website: https://openfoam.org
  \\  /    A nd           | Version: 7
   \\/     M anipulation  |
\*---------------------------------------------------------------------------*/

FoamFile {
    version 2.0;
    format ascii;
    class dictionary;
    object controlDict;
}
libs ("libsimpleFunctionObjects.so" "libgroovyBC.so"
"libsimScaleFunctionObjects.so");
functions {
    sigHandler {
        type writeOldTimesOnSignal;
        sleepSecondsBeforeReraising 60;
```

```
    numberOfTimestepsToStore 1;
    writeCurrent false;
    sigFPE true;
    sigSEGV false;
    sigINT false;
    sigQUIT true;
}
flexibleWriter {
    type flexibleWriter;
    clockTimeLimit 60;
    fracTime 0.1;
}
pressureTools0 {
    enabled on;
    outputControl outputTime;
    outputInterval 1;
    log on;
    type pressureTools;
    functionObjectLibs ("libutilityFunctionObjects.so");
    calcCoeff no;
    calcTotal yes;
    resultName (P) Pressure _tot_0;
    pName p;
    UName U;
    rhoName rhoInf;
    rhoInf 1.225;
    pRef 0.0;
}
pressureTools1 {
    enabled on;
    outputControl outputTime;
    outputInterval 1;
    log on;
    type pressureTools;
    functionObjectLibs ("libutilityFunctionObjects.so");
```

```
        calcCoeff yes;
        calcTotal yes;
        resultName (P) cP_C_tot_1;
        pName p;
        UName U;
        rhoName rhoInf;
        rhoInf 1.225;
        pRef 0.0;
        pInf 1.0;
        UInf (50.0 0.0 0.0);
    }
}
application simpleFoam;
startFrom startTime;
stopAt writeNow;
purgeWrite 0;
writeFormat ascii;
writePrecision 12;
writeCompression on;
timeFormat general;
timePrecision 12;
runTimeModifiable yes;
deltaT 1.0;
startTime 0;
endTime 2000.0;
adjustTimeStep no;
writeControl timeStep;
writeInterval 1;
secondaryWriteControl adjustableRunTime;
secondaryWriteInterval 2000.0;
```

C.2 fvSolution

```
/*--------------------------------*- C++ -*----------------------------------*\
=========                 |
\\      /  F ield         | OpenFOAM: Open Source CFD Toolbox
 \\    /   O peration     | Website: https://openfoam.org
  \\  /    A nd           | Version: 7
   \\/     M anipulation  |
\*---------------------------------------------------------------------------*/

FoamFile {
    version 2.0;
    format ascii;
    class dictionary;
    object fvSolution;
}
solvers {
    U {
        solver smoothSolver;
        tolerance 1e-06;
        relTol 0.01;
        smoother GaussSeidel;
    }
    p {
        solver GAMG;
        tolerance 1e-06;
        relTol 0.001;
        smoother GaussSeidel;
        nPreSweeps 2;
        nPostSweeps 1;
        cacheAgglomeration on;
        agglomerator faceAreaPair;
        nCellsInCoarsestLevel 10;
        mergeLevels 1;
```

```
    }
    k {
        solver smoothSolver;
        tolerance 1e-06;
        relTol 0.01;
        smoother GaussSeidel;
    }
    omega {
        solver smoothSolver;
        tolerance 1e-06;
        relTol 0.01;
        smoother GaussSeidel;
    }
}
relaxationFactors {
    fields {
        p 0.3;
    }
    equations {
        U 0.7;
        k 0.3;
        omega 0.3;
    }
}
SIMPLE {
    nNonOrthogonalCorrectors 0;
    pRefCell 0;
    pRefValue 0.0;
    residualControl {
        U 1e-06;
        "p.*" 1e-06;
        k 1e-06;
        omega 1e-06;
    }
}
```

```
potentialFlow {
    nNonOrthogonalCorrectors 5;
    pRefCell 0;
    pRefValue 0.0;
}
```

Bibliography

[1] Physics, R., "Reynolds number." https://www.reactor-physics.com/engineering/fluid-dynamics/laminar-flow-vs-turbulent-flow/. Accessed: March 2020.

[2] White, F. M., *Fluid mechanics*. McGraw-hill, 1999.

[3] Nada, A. A., "Airfoil shape parameters." https://www.researchgate.net/figure/AIRFOIL-SHAPE-PARAMETERS_fig4_267490031. Accessed: April 2020.

[4] Technical, F. ., "Formula 1 aerodynamics - introduction." https://www.f1technical.net/features/21555. Accessed: February 2020.

[5] TotalSimulation, "Secrets of the role of a front wing." https://www.totalsimulation.co.uk/secrets-formula-1-part-3-role-front-wing/. Accessed: January 2020.

[6] Motorsport, "Front wing of the fw 41." https://www.motorsport.com/f1/photos/williams-fw41-front-wing-detail-16567949/36927324/. Accessed: March 2020.

[7] Autosport, "Airflow explained." https://www.autosport.com/f1/news/130957/tech-video-f1-airflow-explained. Accessed: February 2020.

[8] Piola, G., "Formula 1 bargeboards." https://es.motorsport.com/f1/news/tecnica-piola-principales-novedades-2019/4517106/. Accessed: February 2020.

[9] AT, F., "Ferrari sf90: modifica ai turning vanes con l'aggiunta di un profilo alare sulle "branchie" del nosecone," *F1 Analisis Tecnica*, vol. 1, no. 1, pp. 1–3, 2019.

[10] Motorsport, "W09 sidepod." https://nl.motorsport.com/f1/photos/mercedes-amg-f1-w09-sidepods-16867301/38024251/. Accessed: March 2020.

[11] Zhang, X., Toet, W., and Zerihan, J., "Ground effect aerodynamics of race cars," 2006.

[12] Memoria, F., "Brabham usava "carro-ventilador" e vencia com niki lauda." https://globoesporte.globo.com/motor/formula-1/blogs/f1-memoria/post/2018/06/17/. Accessed: March 2020.

[13] Reddit, "F1 floor." https://www.reddit.com/r/formula1/comments/6nzp31/floor_of_mercedes_amg_at_silverstone_picture_f1s/. Accessed: March 2020.

[14] Motorsport, "Detalle del difusor trasero red bull racing rb14." https://es.motorsport.com/f1/photos/detalle-del-difusor-trasero-red-bull-racing-rb14-16062352/33190900/. Accessed: March 2020.

[15] Motor1, "Diffuser ban." https://www.motor1.com/news/21731/diffuser-ban-to-make-f1-cars-two-seconds-slower/. Accessed: March 2020.

[16] Katz, J., *Race Car Aerodynamics*. Bentley Publishers, Cambridge, third ed., 2006.

[17] Motorsport, "Wingtip vortices." https://www.motorsport.com/f1/photos/lewis-hamilton-mclaren-mercedes-and-his-rear-wing-causing-a-2/1073836/. Accessed: March 2020.

[18] ESPN, "Busting the myth of brawn gp." https://www.espn.com/f1/story/_/id/28167450/busting-myth-brawn-gp-legendary-double-diffuser. Accessed: March 2020.

[19] Gate, R., "Naca 0012." https://www.researchgate.net/figure/NACA0012-airfoil-structured-unstretched-mesh-16K-grid-nodes_fig28_272292649. Accessed: April 2020.

[20] SU2Code, "Naca 0012." https://su2code.github.io/tutorials/Inviscid_2D. Accessed: April 2020.

[21] Gate, R., "Naca 0012." https://www.researchgate.net/figure/Hybrid-Grid-with-structured-prism-layer-mesh-around-the-airfoil. Accessed: April 2020.

[22] Gate, R., "Rans." https://www.researchgate.net/figure/Turbulence-kinetic-energy-around-the-airfoil-and-in-the-wake-region. Accessed: April 2020.

[23] Zhai, Z. J., Zhang, Z., Zhang, W., and Chen, Q. Y., "Evaluation of various turbulence models in predicting airflow and turbulence.," *Hvac&R Research*, vol. 13, no. 6, pp. 853–870, 2007.

[24] Finnemore, E. J., Franzini, J. B., *et al.*, *Fluid mechanics with engineering applications*, vol. 10. McGraw-Hill New York, 2002.

[25] Wikipedia, "Turbulent flows." https://es.wikipedia.org/wiki/Flujo_turbulento. Accessed: March 2020.

[26] Schlichting, H. and Gersten, K., *Boundary-layer theory*. Springer, 2016.

[27] Wikipedia, "Continuity equation." https://en.wikipedia.org/wiki/Continuity_equation#Fluid_dynamics. Accessed: April 2020.

[28] Batchelor, G., *Introduccion a la Dinamica de Fluidos*. Ministerio de Medio Ambiente. Dirección General del Instituto Nacional de . . . , 1997.

[29] Winiecki, T., McCann, J., and Adams, C., "Pressure drag in linear and non-linear quantum fluids," *Physical review letters*, vol. 82, no. 26, p. 5186, 1999.

[30] NASA, "Wrong lift production." https://www.grc.nasa.gov/WWW/K-12/airplane/wrong1.html. Accessed: April 2020.

[31] Wikipedia, "Downwash." https://en.wikipedia.org/wiki/Downwash. Accessed: April 2020.

[32] Framework, F., "What is coanda effect and its use in formula 1." http://f1framework.blogspot.com/2012/03/what-is-coanda-effect-and-its-use-in.html. Accessed: March 2020.

[33] Wright, P. and Matthews, T., *Formula 1 technology*. SAE, 2001.

[34] Newey, A., *How to build a car*. Harper Collins, UK, second ed., 2017.

[35] Throttle, C., "7 tiny aero bits." https://www.carthrottle.com/post/w8y53x3/, Accessed: February 2020.

[36] Elacelerador, "Outwash effect." https://elacelerador.com/alerones-2019-efecto-outwash/. Accessed: March 2020.

[37] Kellar, W., Pearse, S., and Savill, A., "Formula 1 car wheel aerodynamics," *Sports Engineering*, vol. 2, no. 4, pp. 203–212, 1999.

[38] Drivetribe, "Aerodynamics of a f1 wheel." https://drivetribe.com/p/aerodynamics-of-an-f1-wheel-UtKr9Px0SIu6XHWuKOL-kA?iid=dqE_z7n4S7m6G8LpzACVKA. Accessed: January 2020.

[39] Rodríguez, A., "Bargeboards: Technical analysis," *Albrod F1*, vol. 2, no. 4, pp. 2–3, 2014.

[40] Wikipedia, "Bargeboards." https://en.wikipedia.org/wiki/Bargeboard_(aerodynamics). Accessed: February 2020.

[41] Atmosphere, F., "Sidepod." https://www.formula1atmosphere.com/aerodinamica/ponton-sidepod/. Accessed: March 2020.

[42] Jenkins, M. and Floyd, S., "Trajectories in the evolution of technology: A multi-level study of competition in formula 1 racing," *Organization studies*, vol. 22, no. 6, pp. 945–969, 2001.

[43] Agathangelou, B. and Gascoyne, M., "Aerodynamic design considerations of a formula 1 racing car," tech. rep., SAE Technical Paper, 1998.

[44] Toet, W., "Aerodynamics and aerodynamic research in formula 1," *The Aeronautical Journal*, vol. 117, no. 1187, pp. 1–26, 2013.

[45] Dictionary, F., "Diffuser." http://www.formula1-dictionary.net/diffuser.html. Accessed: March 2020.

[46] Engineering, V., "Diffusers." https://www.verus-engineering.com/blog/informative-8/post/diffusers-how-they-work-53. Accessed: March 2020.

[47] Senior, A. E., *The aerodynamics of a diffuser equipped bluff body in ground effect*. PhD thesis, University of Southampton, 2002.

[48] Yokomaku, H., "Rear wing for an automobile," June 8 2004. US Patent App. 29/172,361.

[49] Babinsky, H., "How do wings work?," *Physics Education*, vol. 38, no. 6, p. 497, 2003.

[50] Hoerner, S. F. and Borst, H. V., "Fluid-dynamic lift, practical information on aerodynamic and hydrodynamic lift," tech. rep., BORST (HENRY V) AND ASSOCIATES WAYNE PA, 1975.

[51] Constantin, P. and Foias, C., *Navier-stokes equations*. University of Chicago Press, 1988.

[52] Eymard, R., Gallouët, T., and Herbin, R., "Finite volume methods," *Handbook of numerical analysis*, vol. 7, pp. 713–1018, 2000.

[53] Versteeg, H. K. and Malalasekera, W., *An introduction to computational fluid dynamics: the finite volume method*. Pearson education, 2007.

[54] Castilla, R., "Introduction to cfd." https://atenea.upc.edu/pluginfile.php/3059914/course/section/556320/IntroductionToCFD.pdf. Accessed: April 2020.

[55] Katz, A. and Sankaran, V., "Mesh quality effects on the accuracy of cfd solutions on unstructured meshes," *Journal of Computational Physics*, vol. 230, no. 20, pp. 7670–7686, 2011.

[56] CFDSupport, "Mesh quality." https://www.cfdsupport.com/OpenFOAM-Training-by-CFD-Support/node131.html. Accessed: April 2020.

[57] Castilla, R., "Turbulence modeling." https://atenea.upc.edu/pluginfile.php/3198843/mod_resource/content/1/TurbulenceModeling.pdf. Accessed: April 2020.

[58] Wilcox, D. C. *et al.*, *Turbulence modeling for CFD*, vol. 2. DCW industries La Canada, CA, 1998.

[59] Perrin, N., "F1 2017 fia specification car." https://perrinn.com/login. Accessed: April 2020.

[60] Ravelli, U. and Savini, M., "Aerodynamic simulation of a f1 car," *Journal of Traffic and Transportation Engineering*, vol. 6, pp. 155–163, 2018.

[61] Celik, I. B., Ghia, U., Roache, P. J., Freitas, C. J., Coleman, H., Raad, P. E., Celik, Ì., Freitas, C., and Coleman, H., "Procedure for estimation and reporting of uncertainty due to discretization in {CFD} applications," 2008.

[62] Online, C., "Turbulent length scale." https://www.cfd-online.com/Wiki/Turbulent_length_scale. Accessed: April 2020.

[63] Online, C., "Turbulent intensity." https://www.cfd-online.com/Wiki/Turbulence_intensity. Accessed: April 2020.

[64] PERRIN, "F1 reference data." https://docs.google.com/spreadsheets/d/1POHSdkdfXeUEeGgh-meufNzVRUycCLvzUfn_TVXs_PE/edit. Accessed: February 2020.

[65] Wikipedia, "Aspect ratio." https://en.wikipedia.org/wiki/Aspect_ratio_(aeronautics). Accessed: April 2020.

[66] Slideshare, "Vorticity." https://slideplayer.es/slide/13178976/. Accessed: April 2020.

[67] One, F., "2021 rules." https://www.formula1.com/en/latest/article.2021-f1-rules-the-key-changes-explained.2dCtCkxNofk20K1B4rJwTk.html. Accessed: April 2020.

[68] Gate, R., "Spalart-allmaras aero." https://www.researchgate.net/post/Why_is_the_Spalart-Allmaras_model_preferred_in_aerodynamics. Accessed: May 2020.

[69] Mcbeath, S., "Follow the leader," *Racecar Engineering*, 2007.

[70] BleacherReport, "Turbulence dumbing." https://bleacherreport.com/articles/220724-f1-turbulence-dumbing-it-down. Accessed: May 2020.

[71] FIA, "Formula 1's 2021 car in the wind tunnel." https://www.youtube.com/watch?v=sn2eisHLwwk. Accessed: May 2020.